IEEE Access
Multidisciplinary | Rapid Review | Open Access Journal

Received March 1, 2018, accepted April 23, 2018, date of publication May 4, 2018, date of current version June 5, 2018.

Digital Object Identifier 10.1109/ACCESS.2018.2833199

Material-by-Design Synthesis of Conformal Miniaturized Linear Phased Arrays

MARCO SALUCCI[1], (Member, IEEE), GIACOMO OLIVERI[1], (Senior Member, IEEE), NICOLA ANSELMI[1], (Member, IEEE), AND ANDREA MASSA[1,2], (Fellow, IEEE)

[1]ELEDIA Research Center, ELEDIA@UniTN-University of Trento, 38123 Trento, Italy
[2]ELEDIA Research Center, ELEDIA@UC3M-Universidad Carlos III de Madrid, 28911 Leganés, Spain

Corresponding author: Andrea Massa (andrea.massa@unitn.it)

This work benefited from the networking activities carried out within the Càtedra de Excelencia UC3M-Santander funded by the Universidad Carlos III de Madrid (Spain) (Prof. A. Massa) and the FET Open CSA PROJECT NANOARCHITECTRONICS (Grant Agreement n. 737135) funded by the EU in the framework of the Horizon 2020 - the Framework Programme for Research and Innovation (2014-2020).

ABSTRACT In this paper, the design of high performance conformal radiating structures is addressed within the Material-by-Design (*MbD*) paradigm. Toward this end, a new synthesis technique based on the innovative integration of a generalized quasi-conformal transformation optics and a source inversion procedure is proposed to fit linear phased arrays to smaller and arbitrarily-shaped surfaces. To the best of our knowledge, it is the first time that a design methodology simultaneously achieves (*i*) a simplification of the antenna layout through the reduction of its aperture and number of elements and (*ii*) its conformal transformation in order to match the aerodynamics of the hosting structure without affecting the required radiation features. It is worth remarking that the synthesized architectures are not only conformal, but they also provide the same performances of larger and straight layouts that could not be directly fitted to the available support. Some representative results are shown and discussed in order to validate the effectiveness of the proposed *MbD* methodology, as well as to highlight its current limitations.

INDEX TERMS Linear array conformal miniaturization, material-by-design (MbD), generalized quasi-conformal transformation optics (QCTO), source inversion (SI).

I. INTRODUCTION AND MOTIVATION

When dealing with the design of modern phased arrays, matching the desired radiation performance (e.g., in terms of sidelobe level, half-power beamwidth, and directivity) is a big challenge in those applications where the size of the antenna is strongly limited by space and weight constraints [1]–[3]. Moreover, the synthesis complexity further increases whether the radiating system must be mounted over a non-regular surface with arbitrary profile (e.g., in case of air/satellite-borne devices) [2], [4]. As a matter of fact, reducing the array aperture and - possibly - the number of elements in the beamforming network (*BFN*) is often for such scenarios a necessary but not sufficient condition to match specific aerodynamic targets. Many unconventional architectures have been proposed for addressing the antenna miniaturization problem [2]. Within this framework, several works deal with the synthesis of compact layouts with the same number of transmit/receive modules (*TRM*s) but arranged in smaller apertures [5]–[7]. Alternatively, smaller size and lower weight antennas are achieved through thinning strategies [2]–[11] aimed at reducing the total number of elements on a uniform lattice. Many optimization techniques based on stochastic [8], [12], analytic [10], [11], or hybrid [13] approaches have been proposed to synthesize such architectures trying to tackle the unavoidable increase of the sidelobes [2]. On the other hand, the design of sparse arrays [14]–[18] allows to achieve more flexible arrangements by considering the location of each *TRM* as an additional degree-of-freedom (*DoF*). Unfortunately, sub-optimal beamforming capabilities are often achieved by such designs due to the reduction of control points [2].

Recently, the introduction of artificially engineered materials (i.e., exhibiting properties not available in nature) opened a completely new (and still widely unexplored) way to design modern electromagnetic (*EM*) devices [19]–[24]. Indeed, reformulating the antenna synthesis problem within the so-called Material-by-Design (*MbD*) paradigm [25]–[29] enables the unprecedented exploitation of materials as a

powerful *DoF* to match user-defined goals. Within this context, quasi-conformal transformation optics (*QCTO*)-based approaches [3]–[31] have rapidly gained a lot of attention, thanks to their capability in obtaining effective *field manipulating devices* with reduced complexity (e.g., with low anisotropy and smooth distributions) as compared to standard *TO* techniques [22].

Within the plethora of applications, still incredibly growing in number and heterogeneity [3]–[31] , a *QCTO*-based methodology has been presented in [3] to address the miniaturization of linear arrays. However, even if simultaneously enabling the reduction of both the array aperture and the number of elements, such approach is limited to the design of non-conformal structures [3]. As a matter of fact, the synthesized metamaterial lenses have a non-controllable *rectangular* shape whose width is larger or equal to the aperture of the reference layout [3]. Given such a constraint, aerodynamic requirements cannot be always fulfilled, since the designed radiating systems cannot be matched to non-regular surfaces, leading to *unfeasible* architectures.

Even if *QCTO* has been already exploited for the synthesis of conformal antennas [18]–[22], [28], [34], to the authors' best knowledge no solution has been proposed so far to design *conformal* and *miniaturized* arrangements having the same radiation performance of larger and straight layouts that cannot be mounted on the hosting support without breaking its aerodynamics. Accordingly, this work proposes an innovative *MbD* methodology aimed at overcoming the current limitations of state-of-the-art approaches for the synthesis of high performance conformal radiating structures. Towards this end, a generalized *QCTO* approach [28] is exploited to provide the designer the full control of the shape and dimensions of the final array-lens system. Moreover, a source inversion (*SI*)-based strategy [3] is integrated in order to enable (*i*) the reduction of the *TRM*s to mitigate mutual coupling effects in the conformal *dense* layout, as well as (*ii*) the easy *reconfigurability* of the radiated beam shape. From the methodological viewpoint, the main contribution of this work is the generalization of the technique presented in [3] to enable the synthesis of miniaturized architectures fully matched to arbitrary profiles and providing the same radiation performance of larger but unfeasible layouts.

The paper is organized as follows. Section II mathematically formulates the conformal miniaturization problem and describes the proposed *MbD* solution approach. A set of numerical experiments is then discussed in Sect. III in order to carefully analyze the performances of the synthesized arrangements, as well as to highlight the current limitations of the presented methodology. Finally, some conclusions are drawn in Sect. IV.

II. MATHEMATICAL FORMULATION

Let us consider a *reference* linear phased array of N elements in the two-dimensional (*2-D*) plane (x, y), whose

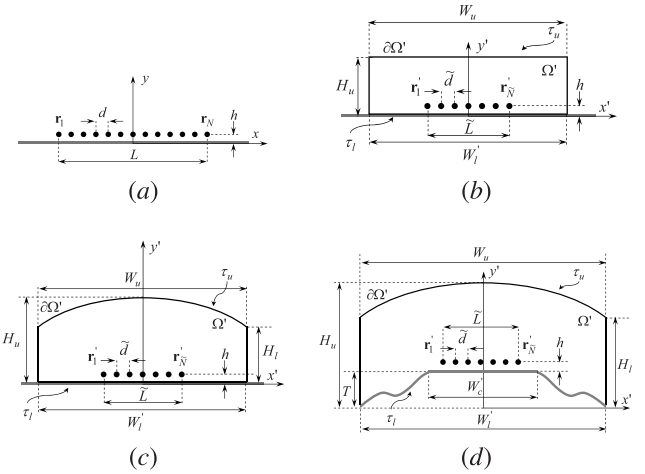

FIGURE 1. ***Problem Geometry*** **- Sketch of (*a*) the *reference* array (i.e., *N d*-spaced elements over a straight metallic ground plane), the miniaturized array with (*b*) a non-conformal/non-aerodynamic (rectangular) lens, (*c*) a non-conformal/aerodynamic (curve) lens, and (*d*) a conformal/aerodynamic (curve) lens.**

n-th radiator is located at position

$$\mathbf{r}_n = \left(x_n = -\frac{L}{2} + (n-1)\, d,\; y_n = h \right); \quad n = 1, \ldots, N \tag{1}$$

$L = (N-1)\, d$ being the array aperture, d the uniform inter-element spacing, and h a fixed height from the underlying metallic ground plane [Fig. 1(*a*)]. By neglecting the time dependency factor $\exp(j2\pi ft)$, each element is modeled as a z-oriented electric current line

$$\mathbf{J}_n(\mathbf{r}) = J_n \delta(\mathbf{r} - \mathbf{r}_n)\, \hat{z}; \quad n = 1, \ldots, N \tag{2}$$

where J_n is a complex excitation and δ is the Dirach's delta function.

The number of transmit/receive modules (*TRM*s) in the beamforming network (*BFN*), N, is properly set in order to meet specific performance requirements of the radiating system (e.g., in terms of sidelobe level and beamwidth). However, let us assume that the following two issues arise during the design process:

1) the required aperture, L, is larger than the available space on the hosting structure;
2) such a hosting structure has a *non-regular* surface, modelled through the arbitrary profile τ_l [Fig. 1(*d*)].

Accordingly, suitable antenna miniaturization techniques should be adopted in order to deal with the first problem, by reducing the array dimensions such that it could fit the mechanical support without changing the radiated field. Several techniques have been proposed in the recent scientific literature to solve such a design problem, and among these the method in [3] appears as one of the most promising

candidates.[1] Indeed, such a methodology is based on a two-step approach devoted at (*i*) designing a metamaterial coating radome able to *compress* the array aperture to $\widetilde{L} < L$ and (*ii*) reducing the number of radiators in the obtained *dense* arrangement by properly synthesizing the set of $\widetilde{N} < N$ equi-spaced excitations of the final layout [Fig. 1(*b*)] [3]. Unfortunately, the metamaterial lens synthesized at (*i*) is characterized by a rectangular shape, whose width is larger or equal to the *reference* aperture [3] [i.e., $W_l' \geq L$ - Fig. 1(*b*)]. Given that, exploiting the approach in [3] for addressing the first issue (miniaturization) would certainly lead to a "failure" in solving the second one (conformal transformation), providing an unfeasible non-conformal layout of the final antenna-radome system [Fig. 1(*b*)].

Following this line of reasoning, a more sophisticated approach is required to fulfill the desired performance goals while meeting mechanical and aerodynamic constraints, through the synthesis of a miniaturized and conformal architecture as the one depicted in Fig. 1(*d*). Accordingly, the following two goals must be simultaneously addressed in solving the arising design problem:

1) synthesize the permittivity and permeability distributions $\underline{\underline{\varepsilon}}'(\mathbf{r}')$ and $\underline{\underline{\mu}}'(\mathbf{r}')$ of a metamaterial radome [$\mathbf{r}' = (x', y') \in \Omega'$ - Fig. 2(*d*)] able to compress the array aperture from L to $\widetilde{L} < L$, whose external contour $\partial\Omega'$ is fully controllable, conformal to τ_l, as well as aerodynamic in the upper part [i.e., matching the desired curve τ_u - Fig. 1(*d*)];
2) determine the positions $\widetilde{\mathbf{r}}_n'$ and excitations $\widetilde{J}_n$, $n = 1, \ldots, \widetilde{N}$ ($\widetilde{N} < N$) of the conformal and miniaturized arrangement [Fig. 1(*d*)] such that its radiated field complies with

$$\widetilde{\mathbf{E}}(\mathbf{r}') = \mathbf{E}(\mathbf{r}); \quad \mathbf{r}' = \mathbf{r},\ \mathbf{r}' \notin \Omega',\ \mathbf{r} \notin \Omega \tag{3}$$

where $\mathbf{E}(\mathbf{r})$ denotes the radiated electric field distribution of the *reference* layout [Fig. 1(*a*)].

In (3), Ω describes a fictitious domain in the original (x, y) plane with arbitrary contour $\partial\Omega$ and characterized by permittivity and permeability distributions $\underline{\underline{\varepsilon}}(\mathbf{r}) = \varepsilon_0 \underline{\underline{I}}$ and $\underline{\underline{\mu}}(\mathbf{r}) = \mu_0 \underline{\underline{I}}$, $\underline{\underline{I}}$ being the identity matrix [Fig. 2(*a*)]. The mapping between Ω [Fig. 2(*a*)] and Ω' [Figs. 2(*b*)-2(*c*)] requires the definition of a proper *deformation* operator

$$\mathbf{r}' = \boldsymbol{\chi}(\mathbf{r}) = \left[\chi_x(\mathbf{r}),\ \chi_y(\mathbf{r}),\ \chi_z(\mathbf{r})\right] \quad \mathbf{r}' \in \Omega',\ \mathbf{r} \in \Omega \tag{4}$$

which is able to avoid the generation of unfeasible/unrealizable permittivity and permeability distributions inside Ω' (i.e., $\underline{\underline{\varepsilon}}'(\mathbf{r}')$ and $\underline{\underline{\mu}}'(\mathbf{r}')$ with very high entries and/or very rapid variations). Consequently, a *QCTO* approach is considered to define $\boldsymbol{\chi}(\mathbf{r})$ given its well known property of realizing smooth transformations through the solution of the Laplace equation [28]

$$\nabla^2 \{\boldsymbol{\chi}(\mathbf{r})\} = 0 \quad \mathbf{r} \in \Omega \tag{5}$$

subject to the Dirichlet boundary condition $\boldsymbol{\chi}(\mathbf{r})|_{\mathbf{r} \in \partial\Omega} = \partial\Omega'$. Moreover, it is worth remarking that the considered domains have arbitrary contours (i.e., $\partial\Omega$ and $\partial\Omega'$ are both chosen by the designer - Fig. 2). Accordingly, the generalized *QCTO* approach in [28] is exploited for realizing the desired mapping, implementing $\boldsymbol{\chi}(\mathbf{r})$ as the cascade of two transformations $\widehat{\mathbf{r}} = \boldsymbol{\Phi}(\mathbf{r})$ and $\mathbf{r}' = \boldsymbol{\Psi}(\widehat{\mathbf{r}})$, involving the introduction of an intermediate rectangular domain $\widehat{\Omega}$ [28] and the repeated solution of (5). The permittivity and permeability tensors of the conformal lens ($\mathbf{r}' \in \partial\Omega'$) are then derived

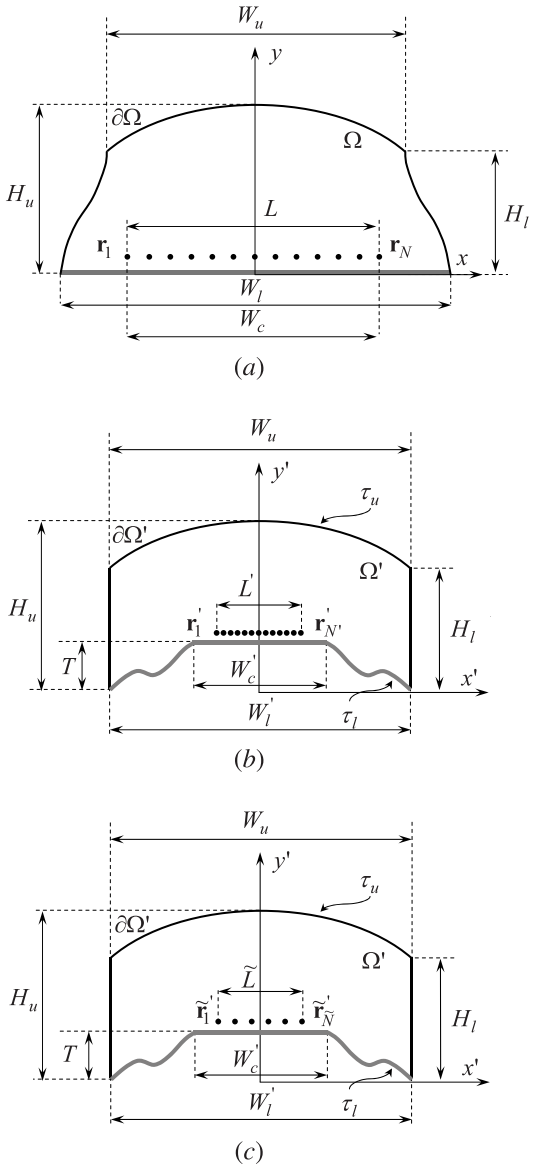

FIGURE 2. ***Problem Geometry ("Circular-Spline" Radome)*** **- Sketch of (*a*) the *reference* layout inside the *fictitious* transformation domain Ω, (*b*) the *QCTO-dense* layout inside the conformal/aerodynamic lens Ω', and (c) the final *QCTO-SI* arrangement.**

[1] It should be pointed out that, although suitable fabrication technologies are currently under investigation for an experimental assessment, the method in [3] appears as a suitable candidate for the problem at hand from a theoretical point of view.

respectively as [28]

$$\underline{\underline{\varepsilon}}'(\mathbf{r}') = \left. \frac{\mathcal{J}[\boldsymbol{\Psi}(\widehat{\mathbf{r}})] \left\{ \frac{\mathcal{J}[\boldsymbol{\Phi}(\mathbf{r})] \underline{\underline{\varepsilon}}(\mathbf{r}) \mathcal{J}^T[\boldsymbol{\Phi}(\mathbf{r})]}{\det\{\mathcal{J}[\boldsymbol{\Phi}(\mathbf{r})]\}} \right|_{\mathbf{r}=\widehat{\mathbf{r}}} \right\} \mathcal{J}^T[\boldsymbol{\Psi}(\widehat{\mathbf{r}})]}{\det\{\mathcal{J}[\boldsymbol{\Psi}(\widehat{\mathbf{r}})]\}} \right|_{\widehat{\mathbf{r}}=\mathbf{r}'} \tag{6}$$

and

$$\underline{\underline{\mu}}'(\mathbf{r}') = \left. \frac{\mathcal{J}[\boldsymbol{\Psi}(\widehat{\mathbf{r}})] \left\{ \frac{\mathcal{J}[\boldsymbol{\Phi}(\mathbf{r})] \underline{\underline{\mu}}(\mathbf{r}) \mathcal{J}^T[\boldsymbol{\Phi}(\mathbf{r})]}{\det\{\mathcal{J}[\boldsymbol{\Phi}(\mathbf{r})]\}} \right|_{\mathbf{r}=\widehat{\mathbf{r}}} \right\} \mathcal{J}^T[\boldsymbol{\Psi}(\widehat{\mathbf{r}})]}{\det\{\mathcal{J}[\boldsymbol{\Psi}(\widehat{\mathbf{r}})]\}} \right|_{\widehat{\mathbf{r}}=\mathbf{r}'} \tag{7}$$

where $.^T$ is the transpose operator, while $\mathcal{J}[\boldsymbol{\zeta}(.)]$ denotes the Jacobian transformation tensor associated to the generic mapping $\boldsymbol{\zeta}(.)$

$$\mathcal{J}[\boldsymbol{\zeta}(.)] = \begin{bmatrix} \frac{\partial \zeta_x(.)}{\partial x} & \frac{\partial \zeta_x(.)}{\partial y} & \frac{\partial \zeta_x(.)}{\partial z} \\ \frac{\partial \zeta_y(.)}{\partial x} & \frac{\partial \zeta_y(.)}{\partial y} & \frac{\partial \zeta_y(.)}{\partial z} \\ \frac{\partial \zeta_z(.)}{\partial x} & \frac{\partial \zeta_z(.)}{\partial y} & \frac{\partial \zeta_z(.)}{\partial z} \end{bmatrix}. \tag{8}$$

It is worth remarking that, given the *2-D* nature of the scenario at hand (Fig. 2), the mapping is independent from the z direction. Accordingly, $\boldsymbol{\chi}(\mathbf{r})$ can be simplified to $\boldsymbol{\chi}(\mathbf{r}) = \boldsymbol{\chi}(x,y) = [\chi_x(x,y), \chi_y(x,y), 1]$, while $\underline{\underline{\varepsilon}}'(\mathbf{r}')$ and $\underline{\underline{\mu}}'(\mathbf{r}')$ have off-diagonal z-entries identically equal to zero (i.e., $\varepsilon'_{xz}(x',y') = \varepsilon'_{yz}(x',y') = \varepsilon'_{zx}(x',y') = \varepsilon'_{zy}(x',y') = 0$ and $\mu'_{xz}(x',y') = \mu'_{yz}(x',y') = \mu'_{zx}(x',y') = \mu'_{zy}(x',y') = 0$ [3]).

Finally, a source inversion (*SI*) strategy [3] is exploited in order to reduce the number of radiators from N to $\widetilde{N} < N$ and restore a uniform spacing $\widetilde{d}$ within the compressed layout [Fig. 2(*c*)]. More precisely, the excitations of the final *QCTO-SI* conformal miniaturized array [with element positions $\widetilde{\mathbf{r}}'_n$, $n = 1, \ldots, \widetilde{N}$ and aperture $\widetilde{L} = (\widetilde{N}-1)\widetilde{d}$ - Fig. 2(*c*)] are determined such that it radiates the same far-field of the *QCTO-dense* layout [Fig. 2(*b*)] when placed in free-space [3]. To achieve such a goal, the *SI* procedure requires the computation of the following expression

$$\widetilde{\mathbf{J}} = \boldsymbol{\mathcal{H}}^{+}\mathbf{F} \tag{9}$$

where $\widetilde{\mathbf{J}} = \{\widetilde{J}_n;\ n = 1, \ldots, \widetilde{N}\}$ is the set of unknown excitations, while

$$\mathbf{F} = \{\mathbf{E}'_0(\mathbf{r}_m);\ m = 1, \ldots, M\} \tag{10}$$

is a collection of M samples of the field radiated in free-space by the *QCTO-dense* arrangement over a properly defined observation domain. Moreover, in (9) $\boldsymbol{\mathcal{H}}^{+}$ is the pseudo-inverse of the $M \times \widetilde{N}$ kernel matrix

$$\boldsymbol{\mathcal{H}} = \left\{ H_0^{(2)}(\mathbf{r}_m \cdot \widetilde{\mathbf{r}}'_n);\ m = 1, \ldots, M;\ n = 1, \ldots, \widetilde{N} \right\} \tag{11}$$

$H_0^{(2)}(.)$ being the second-kind Hankel function of 0-th order and '$\cdot$' denoting the scalar product, computed through a truncated singular value decomposition (*SVD*) operator [3].

For completeness, the proposed design methodology is summarized in the following procedural steps (Fig. 3):

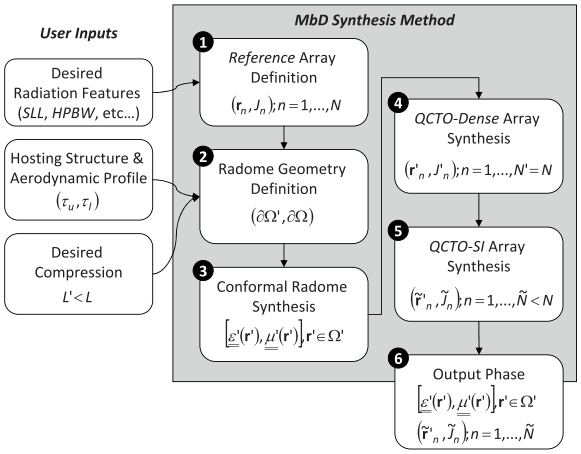

FIGURE 3. Flow chart of the proposed MbD Synthesis method.

1) ***Reference* Array Definition** - Define the *reference* array architecture ($\mathbf{r}_n$, $n = 1, \ldots, N$ and J_n, $n = 1, \ldots, N$) meeting specific performance requirements in terms of radiation features [Fig. 2(*a*)];
2) **Radome Geometry Definition** - Given the arbitrary profile τ_l of the hosting structure and the desired aerodynamic profile τ_u, define the lens shape $\partial\Omega'$ [Fig. 2(*b*)]. Then, set the boundary $\partial\Omega$ of the fictitious domain Ω [Fig. 2(*a*)] such that the desired compression ($L \rightarrow L' < L$) of the *reference* arrangement into the $QCTO-dense$ layout is obtained [Fig. 2(*b*)];
3) **Conformal Radome Synthesis** - Compute the two intermediate transformation rules $\widehat{\mathbf{r}} = \boldsymbol{\Phi}(\mathbf{r})$ and $\mathbf{r}' = \boldsymbol{\Psi}(\widehat{\mathbf{r}})$ defining the overall deformation operator $\mathbf{r}' = \boldsymbol{\chi}(\mathbf{r})$ by numerically solving twice (5) through the generalized *QCTO* method [28]. Then, use (6) and (7) to compute the material distributions inside the conformal lens [i.e., $\underline{\underline{\varepsilon}}'(\mathbf{r}')$ and $\underline{\underline{\mu}}'(\mathbf{r}')$, $\mathbf{r}' \in \Omega'$ - Fig. 2(*b*)];
   For what concerns the transformation of the original sources [Fig. 2(*a*)] into the *QCTO-dense* arrangement [with $N' = N$ elements, aperture $L' < L$, spacing $d' < d$ and profile conformal to τ_l - Fig. 2(*b*)], their excitations are set to $J'_n = J_n$, $n = 1, \ldots, N'$, while the locations are computed as $\mathbf{r}'_n = \boldsymbol{\Psi}[\boldsymbol{\Phi}(\mathbf{r}_n)]$, $n = 1, \ldots, N'$ [Fig. 2(*b*)].
4) ***QCTO-Dense* Array Synthesis** - Set the $N' = N$ excitations of the *QCTO-dense* arrangement to $J'_n = J_n$, $n = 1, \ldots, N'$ and compute their locations inside Ω' as $\mathbf{r}'_n = \boldsymbol{\Psi}(\boldsymbol{\Phi}(\mathbf{r}_n))$, $n = 1, \ldots, N'$ [Fig. 2(*b*)];
5) ***QCTO-SI* Array Synthesis** - Fill the vector $\mathbf{F}$ with M observations of the free-space far-field pattern radiated by the *QCTO-dense* array and the $M \times \widetilde{N}$ kernel matrix $\boldsymbol{\mathcal{H}}$ (11). Then, compute by means of a truncated *SVD* the pseudo-inverse of $\boldsymbol{\mathcal{H}}$, $\boldsymbol{\mathcal{H}}^{+}$, and solve (9) to retrieve the $\widetilde{N} < N$ excitations of the final *QCTO-SI* conformal and miniaturized arrangement [Fig. 2(*c*)];
6) **Output Phase** - Return the material distribution (i.e., $\underline{\underline{\varepsilon}}'(\mathbf{r}')$ and $\underline{\underline{\mu}}'(\mathbf{r}')$, $\mathbf{r}' \in \Omega'$) and the excitations $\widetilde{J}_n$,

$n = 1, \ldots, \widetilde{N}$ of the synthesized conformal and miniaturized structure [Fig. 2(*c*)] behaving as the *reference* antenna [Fig. 2(*a*)].

III. NUMERICAL RESULTS

This section is aimed at numerically assessing the effectiveness, the potentialities, as well as the limitations of the proposed *MbD* methodology for the design of miniaturized and conformal linear phased arrays. Towards this end, full-wave simulations based on the *2D* finite element method (*FEM*) have been exploited. Moreover, in order to measure the "complexity" of the synthesized lenses both the ranges of the permittivity tensors computed through (6) (i.e., $\varepsilon'_{\max} = \max_{\mathbf{r}' \in \Omega'} \left\{ \varepsilon'_{pq} \left(\mathbf{r}' \right) ; \, p, q \in \{x, y, z\} \right\}$ and $\varepsilon'_{\min} = \min_{\mathbf{r}' \in \Omega'} \left\{ \varepsilon'_{pq} \left(\mathbf{r}' \right) ; \, p, q \in \{x, y, z\} \right\}$) and the corresponding average *fractional anisotropy* ($0 \leq \alpha_F \leq 1$) and average *relative anisotropy* ($0 \leq \alpha_R \leq \sqrt{2}$) indexes will be evaluated ($\alpha_F = \alpha_R = 0$ indicating fully isotropic materials [26], [29]). Moreover, the "quality" of the obtained solutions will be measured by computing the following matching error between the far-field pattern radiated by the synthesized *QCTO-SI* (i.e., $\widetilde{E}(\phi)$) and by the *reference* (i.e., $E(\phi)$) arrays

$$\xi = \frac{\int_0^{\pi} \left(\left| \widetilde{E}(\phi) \right| - |E(\phi)| \right)^2 d\phi}{\int_0^{\pi} |E(\phi)|^2 \, d\phi}. \tag{12}$$

As a first numerical benchmark, let us consider a *reference* array of $N = 20$ $d = \frac{\lambda}{2}$-spaced elements ($L = 9.5\lambda$) arranged at a height of $h = \frac{\lambda}{4}$ over a metallic ground plane [Step 1: *Reference Array Definition* - Fig. 2(*a*)]. The goal of the design problem is to reduce the number of control points of such a *reference* configuration [i.e., obtaining $N \rightarrow \widetilde{N} < N$ and $L \rightarrow \widetilde{L} < L$ in the final $QCTO - SI$ layout - Fig. 2(*c*)], while guaranteeing that the synthesized radiating system (*i*) is conformal to the underlying hosting structure [whose profile is modeled by the curve τ_l - Fig. 2(*c*)] as well as (*ii*) exhibits the desired aerodynamic profile [modeled by the curve τ_u - Fig. 2(*c*)]. Accordingly, the external contour of the designed "*Circular-Spline*" radome $\partial\Omega'$ has been set (Step 2: *Radome Geometry Definition*) to the union of the curves τ_l, τ_u, with two vertical segments of length H_l connecting points $\left(\pm \frac{W'_l}{2}, 0 \right)$ and $\left(\pm \frac{W'_l}{2}, H_l \right)$ [$W'_l = 20\lambda$ and $H_l = 8\lambda$ - Fig. 2(*c*)]. The lower profile, τ_l, has been composed by two (arbitrarily-chosen) symmetric spline curves defined for $-\frac{W'_l}{2} \leq x' \leq -\frac{W'_c}{2}$ and $\frac{W'_c}{2} \leq x' \leq \frac{W'_l}{2}$, respectively, and by the horizontal segment connecting points $\left(-\frac{W'_c}{2}, T \right)$ and $\left(\frac{W'_c}{2}, T \right)$ [$W'_c = 8.5\lambda$ and $T = 3\lambda$ - Fig. 2(*c*)]. On the other hand, the upper profile (τ_u) has been defined as the circular arc passing through the points $\left(-\frac{W_u}{2}, H_l \right)$, $(0, H_u)$, and $\left(\frac{W_u}{2}, H_l \right)$ [$W_u = 20\lambda$, $H_u = 11\lambda$ - Fig. 2(*c*)]. Once the desired lens shape has been defined, the boundary $\partial\Omega$ of the fictitious region Ω [Fig. 2(*a*)] has been set in order to obtain

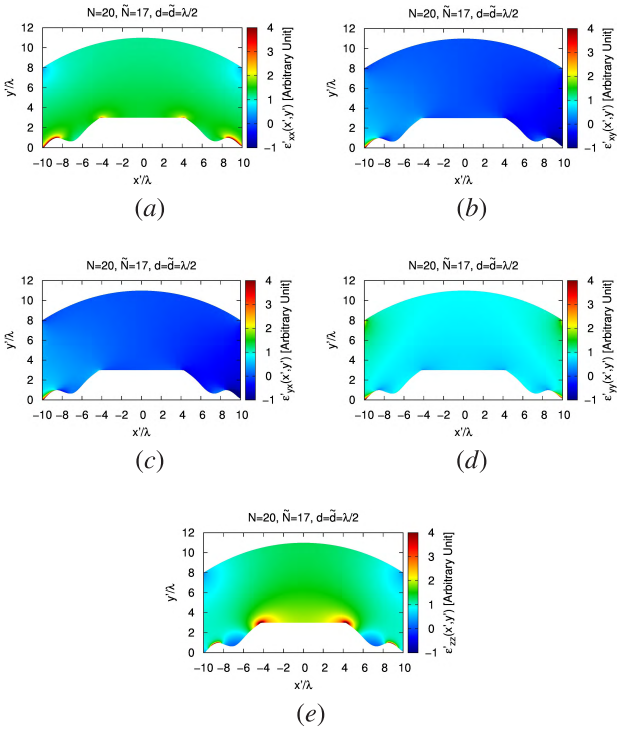

FIGURE 4. ***Numerical Assessment* ("*Circular-Spline*" *Radome*; $N = 20$, $d = \frac{\lambda}{2}$, $N' = 20$, $d' < \frac{\lambda}{2}$, $\widetilde{N} = 17$, $\widetilde{d} = \frac{\lambda}{2}$, $\rho = 0.84$) - Relative permittivity distribution of the *QCTO*-synthesized conformal radome: (*a*) $\varepsilon_{xx}(\mathbf{r}')$, (*b*) $\varepsilon_{xy}(\mathbf{r}')$, (*c*) $\varepsilon_{yx}(\mathbf{r}')$, (*d*) $\varepsilon_{yy}(\mathbf{r}')$, and (e) $\varepsilon_{zz}(\mathbf{r}')$.**

a desired compression of the *reference* array into a smaller (and conformal to τ_l) arrangement made of $\widetilde{N} = 17$ elements (i.e., providing $\widetilde{L} = 8\lambda$ and $\rho = \frac{\widetilde{L}}{L} = 0.84$). Towards this end, the left and right hand sides of $\partial\Omega$ have been defined as follows [Fig. 2(*a*)]

$$\begin{cases} x = \left(\dfrac{W_l - W_u}{4} \right) \left[\cos\left(\dfrac{\pi y}{H_l} \right) + 1 \right] + \dfrac{W_u}{2} \\ \qquad x > 0, \; y \in [0, \, H_l] \\ x = -\left(\dfrac{W_l - W_u}{4} \right) \left[\cos\left(\dfrac{\pi y}{H_l} \right) + 1 \right] - \dfrac{W_u}{2} \\ \qquad x < 0, \; y \in [0, \, H_l] \, . \end{cases} \tag{13}$$

where the value of W_l (which controls the degree of compression of the *reference* elements) has been empirically set to $W_l = 20.5\lambda$ in order to achieve the desired miniaturization.

The relative electric permittivity distribution inside the synthesized lens (i.e., the non-null entries of $\underline{\underline{\varepsilon}}'(\mathbf{r}')$, for $\mathbf{r}' \in \Omega'$) computed by means of (6) is shown in Fig. 4 (Step 3: *Conformal Radome Synthesis*)[2]. As it can be observed, the off-diagonal entries of $\underline{\underline{\varepsilon}}'(\mathbf{r}')$ [i.e., $\varepsilon'_{xy}(\mathbf{r}')$ - Fig. 4(*b*) and $\varepsilon'_{yx}(\mathbf{r}')$ - Fig. 4(*c*)] have equal distributions and values close to zero almost everywhere within Ω'. On the contrary, larger variations characterize the diagonal entries

[2]Given the symmetry of (6) and (7), the permeability tensor $\underline{\underline{\mu}}'(\mathbf{r}')$ exhibits the same spatial distribution of $\underline{\underline{\varepsilon}}'(\mathbf{r}')$ and for such a reason it is not reported.

TABLE 1. ***Numerical Assessment*** **(*"Circular-Spline" Radome*; $N = 20$, $d = \frac{\lambda}{2}$, $N' = 20$, $d' < \frac{\lambda}{2}$, $\widetilde{N} = 17$, $\widetilde{d} = \frac{\lambda}{2}$, $\rho = 0.84$) - Performance indexes, lens features, and excitations indicators for the *reference*, *QCTO-dense*, and *QCTO-SI* layouts.**

	Reference Array	*QCTO-dense* Array		*QCTO-SI* Array
		No Radome	Radome	
N	20	20	20	17
L	9.5λ	8.0λ	8.0λ	8.0λ
ξ	-	1.22×10^{-1}	1.66×10^{-2}	1.77×10^{-2}
SLL [dB]	13.19	14.83	12.33	12.09
β_{SLL} [%]	-	12.43	-6.52	-8.34
$HPBW$ [deg]	5.07	6.38	4.95	5.05
β_{HPBW} [%]	-	25.84	-2.37	-0.39
$[\varepsilon'_{\min}, \varepsilon'_{\max}]$	-	-	$[-4.62, 13.33]$	$[-4.62, 13.33]$
α_F	-	-	3.26×10^{-1}	3.26×10^{-1}
α_R	-	-	3.10×10^{-1}	3.10×10^{-1}
DRR	1.0	1.0	1.0	1.08

[i.e., $\varepsilon'_{xx}(\mathbf{r}')$ - Fig. 4(a), $\varepsilon'_{yy}(\mathbf{r}')$ - Fig. 4(d), and $\varepsilon'_{zz}(\mathbf{r}')$ - Fig. 4(e)] especially in correspondence to the lower region, which is subject to an higher deformation to match the profile τ_l. However, it is worth pointing out that the permittivity values are always bounded in the range $[\varepsilon'_{\min}, \varepsilon'_{\max}] = [-4.62, 13.33]$ (Fig. 4 and Tab. 1), which is compatible with recent metamaterials design and fabrication processes [35], [36]. Moreover, the synthesized material is characterized by a limited anisotropy despite the non-negligible deformation occurring between $\partial\Omega$ and $\partial\Omega'$ [Fig. 2(a) vs. Fig. 2(c)], as denoted by the computed anisotropy indexes (i.e., $\alpha_F = 3.26 \times 10^{-1}$ and $\alpha_R = 3.10 \times 10^{-1}$ - Tab. 1).

Leaving for later discussion the analysis of the radiated far-field patterns, to preliminary verify the effectiveness of the *QCTO*-synthesized lens Figure 5 shows the simulated near-field distribution after applying the computed transformation operator to map the original $N = 20$ radiators inside Ω' (i.e., letting $\mathbf{r}'_n = \boldsymbol{\Psi}(\boldsymbol{\Phi}(\mathbf{r}_n))$, $n = 1, \ldots, N' = N$ - Step 4: *QCTO-Dense* Array Synthesis).

As it can be observed, the synthesized conformal/aerodynamic metamaterial covering allows the $QCTO-dense$ arrangement (having $N' = 20$ elements with spacing $d' < \frac{\lambda}{2}$ since $L' = \widetilde{L} = 8\lambda < L$) to radiate outside $\partial\Omega'$ almost the same field distribution of the *reference* array [i.e., Fig. 5(d) vs. Fig. 5(a)], as pointed out by the magnitude of the difference field [i.e., $\bigtriangleup E_z(\mathbf{r})\big|_{QCTO-dense} = [E_z(\mathbf{r}) - E'_z(\mathbf{r})]$ - Fig. 5(e)][3].

As a matter of fact, a visible mismatch with respect to the *reference* distribution can be observed when removing the synthesized lens [i.e., considering the "no-radome" $QCTO - dense$ layout - Fig. 5(b) vs. Fig. 5(a), and the magnitude of the difference field shown in Fig. 5(c)].

Going through the steps of the proposed *MbD* synthesis methodology (Sect. II), let us now analyze the features

[3]It should be pointed out that $E'_z(\mathbf{r}) = E_z[\boldsymbol{\Psi}(\boldsymbol{\Phi}(\mathbf{r}))] = E_z(\mathbf{r})$ when $\mathbf{r} \notin \Omega'$ because $\boldsymbol{\Psi}(\boldsymbol{\Phi}(\mathbf{r})) = \mathbf{r}$, while $E'_z(\mathbf{r}) \neq E_z(\mathbf{r})$ for $\mathbf{r} \in \Omega'$ because $\boldsymbol{\Psi}(\boldsymbol{\Phi}(\mathbf{r})) \neq \mathbf{r}$.

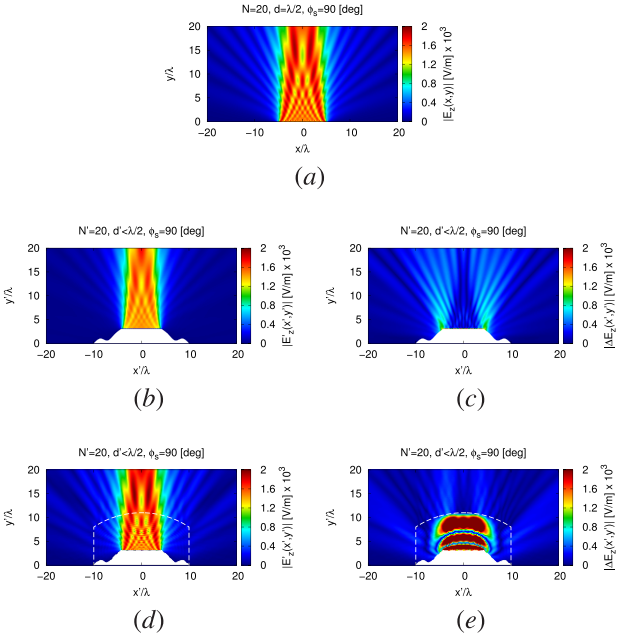

FIGURE 5. ***Numerical Assessment*** **(*"Circular-Spline" Radome*; $N = 20$, $d = \frac{\lambda}{2}$, $N' = 20$, $d' < \frac{\lambda}{2}$, $\widetilde{N} = 17$, $\widetilde{d} = \frac{\lambda}{2}$, $\rho = 0.84$; $\phi_s = 90$ [deg]) - Magnitude of the near-field radiated by (a) the *reference* array and by the *QCTO-dense* array (b) without and (d) with radome; magnitude of the near-field difference between the *reference* distribution and the *QCTO-dense* array (c) without and (e) with radome.**

of the final conformal and miniaturized radiating system having a lower number of equally-spaced radiators (i.e., $\widetilde{N} = 17$, $\widetilde{d} = \frac{\lambda}{2}$ - Step 5: *QCTO-SI Array Synthesis*). Figure 6 shows the outcome of the *SI* procedure, by comparing the magnitude [Fig. 6(a)] and phase [Fig. 6(b)] of the excitations of the *reference* layout (i.e., J_n, $n = 1, \ldots, N$) with those of the *QCTO-SI* array [i.e., $\widetilde{J}_n$, $n = 1, \ldots, \widetilde{N}$, computed through (9)]. Interestingly, even if the *SI*-synthesized excitations are not uniform despite the broadside steering of the main beam [Fig. 5(a)], they exhibit a quite low dynamic range ratio (DRR) according to the reference literature [37], [38], being

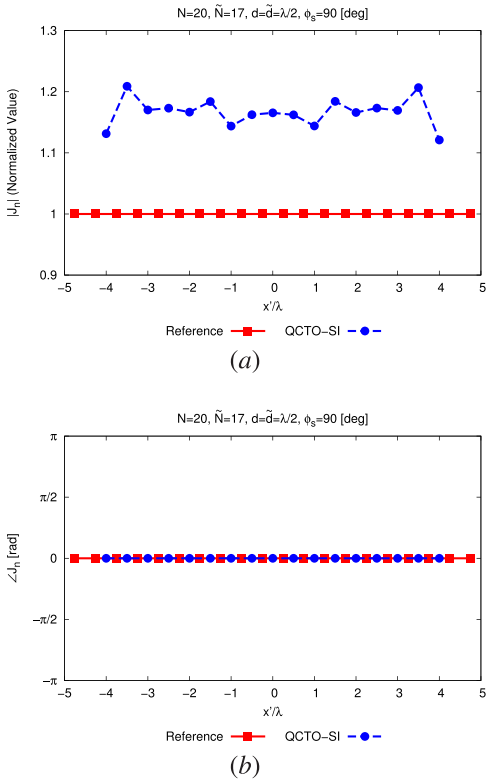

FIGURE 6. ***Numerical Assessment*** **(*"Circular-Spline" Radome*; $N = 20$, $d = \frac{\lambda}{2}$, $N' = 20$, $d' < \frac{\lambda}{2}$, $\tilde{N} = 17$, $\tilde{d} = \frac{\lambda}{2}$, $\rho = 0.84$; $\phi_S = 90$ [deg]) - Distribution of (*a*) the amplitudes (i.e., $|J_n|$, $n = 1, \ldots, N$, and $\left|\tilde{J}_n\right|$, $n = 1, \ldots, \tilde{N}$) and (*b*) the phases (i.e., $\angle J_n$, $n = 1, \ldots, N$, and $\angle \tilde{J}_n$, $n = 1, \ldots, \tilde{N}$) of the *reference* and *QCTO-SI* arrangements.**

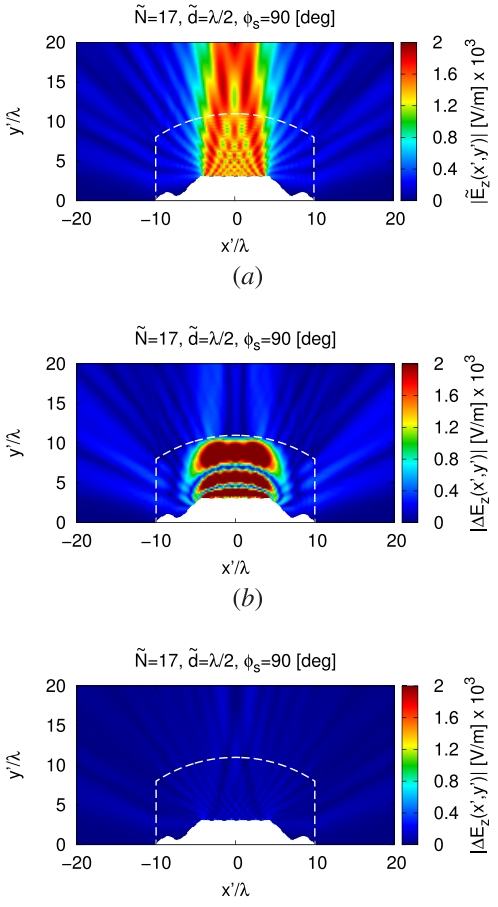

FIGURE 7. ***Numerical Assessment*** **(*"Circular-Spline" Radome*; $N = 20$, $d = \frac{\lambda}{2}$, $N' = 20$, $d' < \frac{\lambda}{2}$, $\tilde{N} = 17$, $\tilde{d} = \frac{\lambda}{2}$, $\rho = 0.84$; $\phi_S = 90$ [deg]) - Magnitude of (*a*) the near-field radiated by the *QCTO-SI* array, (*b*) the near-field difference between the *QCTO-SI* and the *reference* distributions, and (*c*) the near-field difference between the *QCTO-SI* and the *QCTO-dense* distributions. .**

equal to $DRR|_{QCTO-SI} = \frac{\max_{n=1,\ldots,\tilde{N}}|\tilde{J}_n|}{\min_{n=1,\ldots,\tilde{N}}|\tilde{J}_n|} = \frac{\tilde{J}_{\max}}{\tilde{J}_{\min}} = 1.08$ [Fig. 6(*a*) and Tab. 1]. As it can be seen by looking at the plots in Fig. 7, the designed $QCTO - SI$ arrangement is able to mimic the field distribution radiated by the *reference* layout [Fig. 7(*a*) vs. Fig. 5(*a*), the magnitude of the difference field $\bigtriangleup E_z(\mathbf{r})\big|_{QCTO-SI} = \left[E_z(\mathbf{r}) - \tilde{E}_z(\mathbf{r})\right]$ being shown in Fig. 7(*b*)]. Such a result confirms the effectiveness of the *SI* step in reducing the number of control points without introducing alterations of the radiation characteristics, as indicated by the difference plot between the $QCTO-dense$ [$N' = N = 20$ - Fig. 5(*d*)] and the $QCTO - SI$ [$\tilde{N} = 17$ - Fig. 7(*a*)] distributions reported in Fig. 7(*c*).

Of course, an evaluation of the actual performance of the proposed synthesis methodology requires a careful analysis of the far-field radiation features of the $QCTO - SI$ array, in order to verify if it is able to match the desired (*reference*) properties. Towards this end, Figure 8 shows the normalized power pattern radiated by the *reference*, the $QCTO - dense$, and the $QCTO - SI$ arrangements. As it can be observed, a very good matching is obtained as quantitatively verified by the computed values of the matching error (i.e., $\xi|_{QCTO-dense} = 1.66 \times 10^{-2}$ and $\xi|_{QCTO-SI} = 1.77 \times 10^{-2}$ - Tab. 1). Besides the very low value of ξ, the good agreement between the $QCTO - SI$ and the *reference* pattern can be further verified by looking at the relative variation of key-indicators such as the sidelobe level (SLL) and half-power beamwidth ($HPBW$)

$$\beta_q = \frac{\left(q - q|_{reference}\right)}{q|_{reference}} \times 100$$
$$q = \{SLL;\ HPBW\} \tag{14}$$

which turn out to be equal to $\beta_{SLL}|_{QCTO-SI} = -8.34\%$ and $\beta_{HPBW}|_{QCTO-SI} = -0.39\%$, respectively (Tab. 1). Unfortunately, a slight degradation of the SLL occurs, even if such a discrepancy is quite limited (i.e., $\frac{SLL|_{QCTO-SI}}{SLL|_{reference}} \approx 0.92$ - Fig. 7 and Tab. 1). Besides the unavoidable errors related to the numerical solution of the $QCTO$ step (requiring the discretization of the transformation domains Ω and Ω'), such a degradation is partially due to the truncation effect (or "transformation truncation" [29], [39]) occurring on the external boundary of $\partial\Omega'$ and causing some reflections to arise in correspondence with the lens/free-space interface, as well as a reduced overlap with the *reference* pattern after the third sidelobe. On the other hand, it is worth remarking

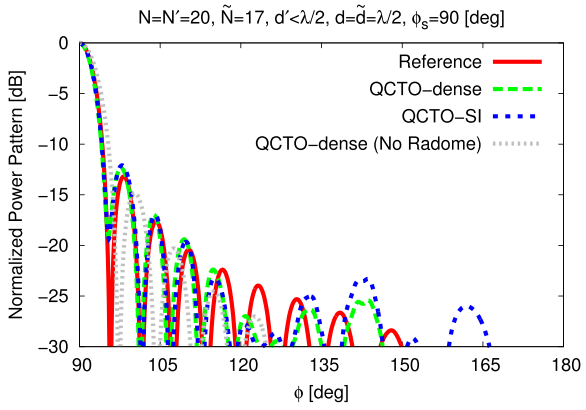

FIGURE 8. ***Numerical Assessment*** **(*"Circular-Spline" Radome*; $N = 20$, $d = \frac{\lambda}{2}$, $N' = 20$, $d' < \frac{\lambda}{2}$, $\tilde{N} = 17$, $\tilde{d} = \frac{\lambda}{2}$, $\rho = 0.84$; $\phi_s = 90$ [deg]) - Power patterns radiated by the *reference* array, the *QCTO-dense* array (with and without radome), and the final *QCTO-SI* layout.**

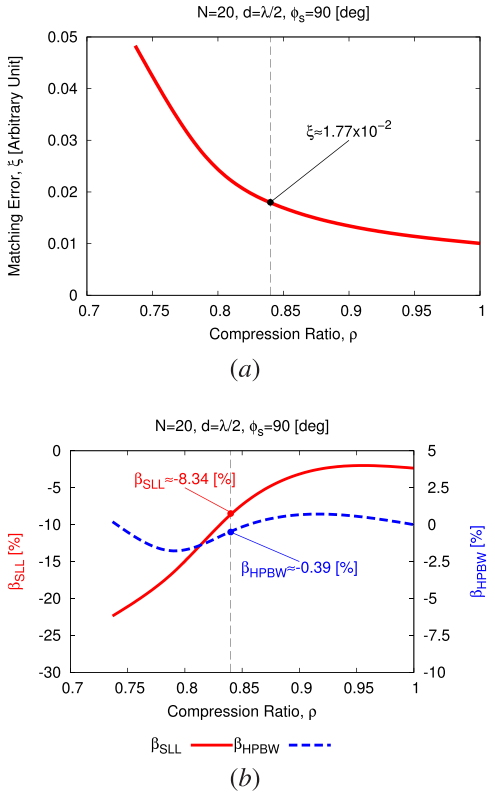

FIGURE 9. ***Numerical Assessment*** **(*"Circular-Spline" Radome*; $N = 20$, $d = \frac{\lambda}{2}$; $\phi_s = 90$ [deg]) - Behaviour of (*a*) the far-field pattern matching error (ξ) and of (*b*) the *SLL* and *HPBW* relative variation (i.e., β_{SLL} and β_{HPBW}) as a function of the array compression ratio ρ.**

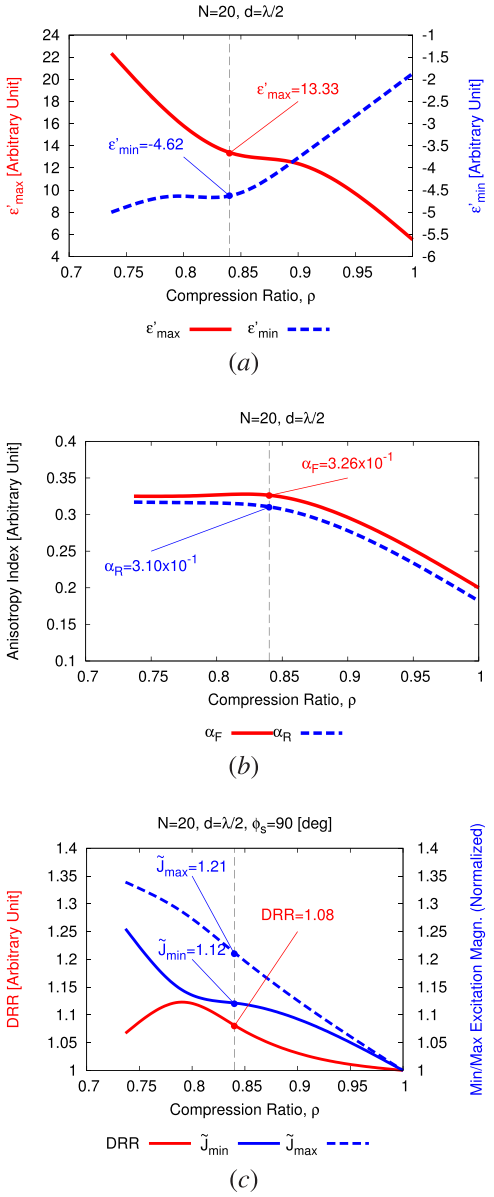

FIGURE 10. ***Numerical Assessment*** **(*"Circular-Spline" Radome*; $N = 20$, $d = \frac{\lambda}{2}$; $\phi_s = 90$ [deg]) - Behavior of (*a*) the bounds of the permittivity tensor (i.e., ε'_{min} and ε'_{max}), (*b*) the anisotropy indexes (i.e., α_F and α_R) of the radome, and (*c*) the descriptors of the synthesized excitations of the *QCTO-SI* array (i.e., $J_{min} = \min_{n=1,\ldots,\tilde{N}} \left|\tilde{J}_n\right|$, $J_{max} = \max_{n=1,\ldots,\tilde{N}} \left|\tilde{J}_n\right|$, and *DRR*) versus the array compression ratio ρ.**

that a significant worsening of the matching is obtained by the $QCTO - dense$ array in the "no-radome" configuration, as denoted by the plot in Fig. 8 and as verified by the corresponding value of the matching error, that increases of about one order of magnitude (i.e., $\xi|^{no-radome}_{QCTO-dense} = 1.22 \times 10^{-1}$ - Tab. 1).

Having assessed the proposed *MbD* methodology on the considered benchmark case, let us now analyze what are the achievable performance when considering different compressions of the *reference* array while matching it to the conformal profile τ_l [Fig. 2(*c*)]. Towards this end, Figure 9(*a*) shows the behaviour of the far-field matching error versus the compression ratio, $\rho = \frac{\tilde{L}}{L}$, between the reference (L) and $QCTO - SI$ ($\tilde{L}$) apertures. It is worth observing that, as expected, lower values of ρ ($\rho < 0.84$) lead to an increase of the matching error, being always $\xi < 5.0 \times 10^{-2}$ even when considering a significant reduction of the control points [i.e., $\xi = 4.83 \times 10^{-2}$ when letting $\tilde{N} = 15, \tilde{L} = 7\lambda, \rightarrow \rho = 0.74$ - Fig. 9(*a*)]. On the other hand, it should be noticed that $\xi \neq 0$ when

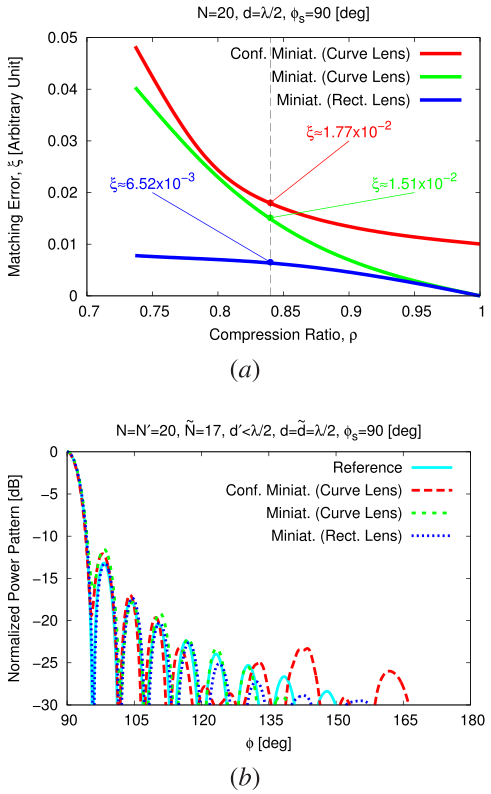

FIGURE 11. ***Numerical Assessment ("Circular-Spline" Radome; $N = 20$, $d = \frac{\lambda}{2}$; $\phi_S = 90$ [deg]) - (a) Behaviour of the matching error (ξ) and as a function of the array compression ratio (ρ) for the conformal miniaturization (curve lens), the miniaturization (curve lens), and the miniaturization (rectangular lens) cases; (b) radiated power patterns by the reference and QCTO − SI arrangements for the different scenarios.***

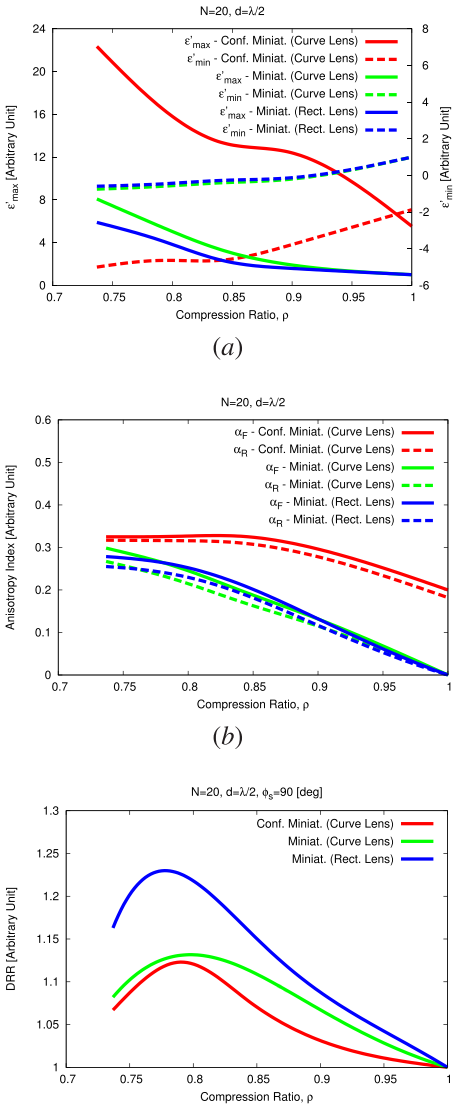

FIGURE 12. ***Numerical Assessment ("Circular-Spline" Radome; $N = 20$, $d = \frac{\lambda}{2}$; $\phi_S = 90$ [deg]) - Behavior of (a) the bounds of the permittivity tensor (i.e., $\varepsilon'_{\min}$ and $\varepsilon'_{\max}$), (b) the anisotropy indexes (i.e., α_F and α_R) of the radome, and (c) the descriptors of the synthesized excitations of the QCTO-SI array (i.e., $J_{\min} = \min_{n=1,\ldots,\tilde{N}} \left|\tilde{J}_n\right|$, $J_{\max} = \max_{n=1,\ldots,\tilde{N}} \left|\tilde{J}_n\right|$, and DRR) versus the array compression ratio ρ for the conformal miniaturization (curve lens), the miniaturization (curve lens), and the miniaturization (rectangular lens) cases.***

setting $\rho = 1$ (i.e., no compression is applied to the *reference* array) because of the conformal transformation of the ground plane required to match the profile τ_l [Fig. 2(*c*)]. Similar conclusions can be drawn by looking at the behaviour of the normalized differences β_{SLL} and β_{HPBW} reported in Fig. 9(*b*), for completeness. If from the one hand it can be seen that reducing ρ leads to a lower *sensitivity* of the synthesized $QCTO - SI$ pattern [showing slightly lower *SLL* values than the *reference* one], on the other hand a very good *resolution* of the main beam is obtained in all considered cases, as clearly indicated by the trend of β_{HPBW} [being always close to $\beta_{HPBW} = 0\%$ - Fig. 9(*b*)]. Besides analyzing the achievable matching in terms of far-field pattern, it is worth considering what is the actual "cost" of the synthesized systems. Towards this end, Figure 10 reports the "complexity" versus ρ of the obtained metamaterials [both in terms of permittivity ranges - Fig. 10(*a*), and anisotropy indexes - Fig. 10(*b*)] and of the computed excitations through the *SI* procedure [Fig. 10(*c*)]. As expected, lower values of ρ (i.e., larger compressions of the *reference* layout) determine a widening of the lens permittivity ranges, being however always bounded to reasonable [37], [38] values [i.e., $\left[\varepsilon'_{\min}, \varepsilon'_{\max}\right] = [-5.00, 22.35]$ when $\rho = 0.74$ - Fig. 10(*a*)], while the anisotropy appears to be always reduced and close to that of the case with $\rho = 0.84$ [Fig. 10(*b*)]. On the other hand, it should be pointed out that larger compressions do not pay a significant increase of the *DRR* [$1.08 \leq DRR|_{0.74 \leq \rho \leq 1} \leq 1.14$ - Fig. 10(*c*)].

In order to better understand what is the actual "complexity" of the design problem at hand, let us now analyze the achievable results when considering two intermediate (easier but sub-optimal) solutions. Clearly, the easiest solution to perform a compression of the *reference* array is to synthesize a rectangular lens of width $W'_l \geq L$ through the approach in [3] [i.e., yielding the layout in Fig. 1(*b*)]. However, it is worth observing that such a result does not allow to obtain

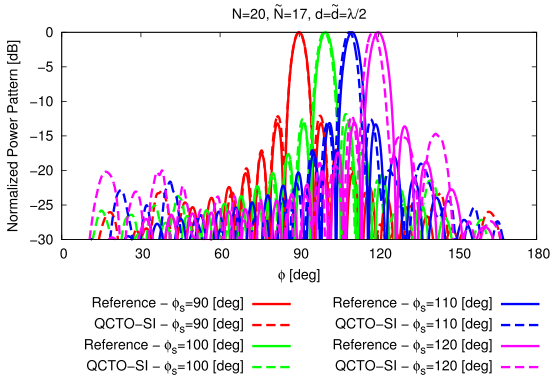

FIGURE 13. *Numerical Assessment ("Circular-Spline" Radome;* $N = 20$, $d = \frac{\lambda}{2}$, $N' = 20$, $d' < \frac{\lambda}{2}$, $\tilde{N} = 17$, $\tilde{d} = \frac{\lambda}{2}$, $\rho = 0.84$) - Power patterns radiated by the *reference* and *QCTO-SI* arrays when considering a steering of the main beam towards the directions $\phi_s = \{90;\ 100;\ 110;\ 120\}$ [deg].

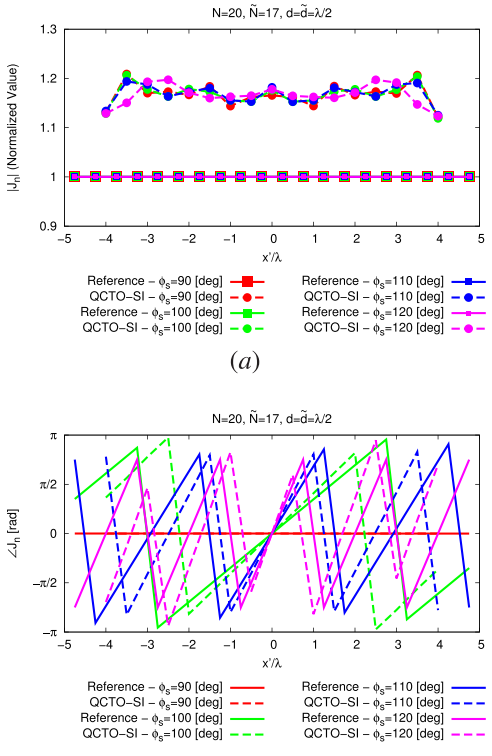

FIGURE 14. *Numerical Assessment ("Circular-Spline" Radome;* $N = 20$, $d = \frac{\lambda}{2}$, $N' = 20$, $d' < \frac{\lambda}{2}$, $\tilde{N} = 17$, $\tilde{d} = \frac{\lambda}{2}$, $\rho = 0.84$) - Distribution of (*a*) the amplitudes (i.e., $|J_n|$, $n = 1, \ldots, N$, and $\left|\tilde{J}_n\right|$, $n = 1, \ldots, \tilde{N}$) and (*b*) the phases (i.e., $\angle J_n$, $n = 1, \ldots, N$, and $\angle \tilde{J}_n$, $n = 1, \ldots, \tilde{N}$) of the *reference* and *QCTO-SI* arrangements when considering a steering of the main beam towards the directions $\phi_s = \{90;\ 100;\ 110;\ 120\}$ [deg].

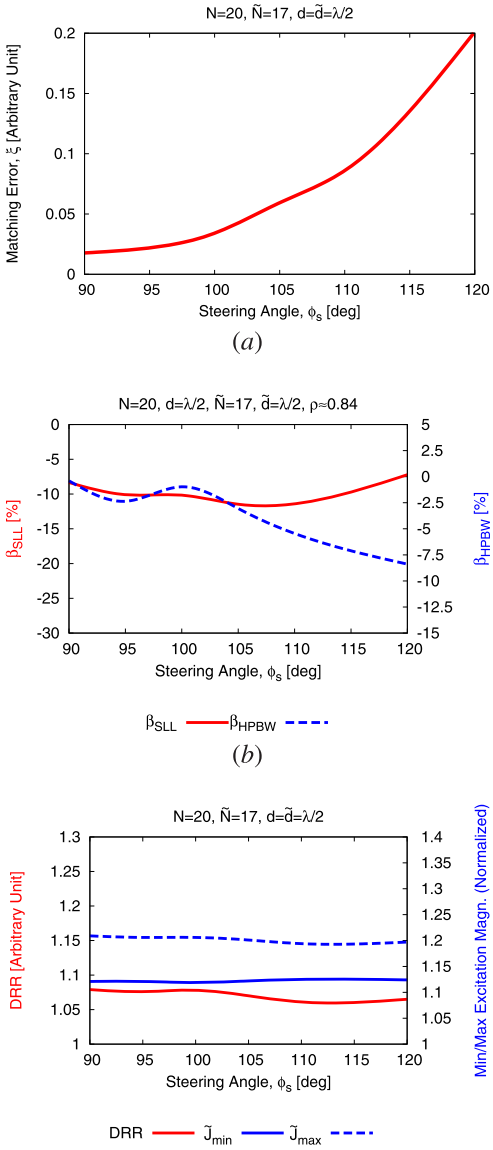

FIGURE 15. *Numerical Assessment ("Circular-Spline" Radome;* $N = 20$, $d = \frac{\lambda}{2}$, $N' = 20$, $d' < \frac{\lambda}{2}$, $\tilde{N} = 17$, $\tilde{d} = \frac{\lambda}{2}$, $\rho \simeq 0.84$) - Behaviour of (*a*) the matching error (ξ), (*b*) the *SLL* and *HPBW* variation (i.e., β_{SLL} and β_{HPBW}), and the descriptors of the synthesized excitations of the *QCTO-SI* array (i.e., $J_{\min} = \min_{n=1,\ldots,\tilde{N}} \left|\tilde{J}_n\right|$, $J_{\max} = \max_{n=1,\ldots,\tilde{N}} \left|\tilde{J}_n\right|$, and *DRR*) as a function of the steering angle ϕ_s.

the desired aerodynamic profile in the upper part, nor the conformal matching to an arbitrarily-shaped structure in the lower part. Thus, an intermediate solution is that of realizing a metamaterial lens that exhibits the desired aerodynamic properties, by curving the upper part in order to fit the profile τ_u [Fig. 1(*c*)]. Unfortunately, such a design would still be sub-optimal, since it does not allow to match a conformal hosting structure, contrarily to what is done through the final design in Fig. 1(*d*). As expected, the miniaturization obtained through a rectangular lens [Fig. 1(*b*)] yields the best performances of the final $QCTO - SI$ layout in terms of far-field matching, as indicated by the plot of ξ versus ρ reported in Fig. 11(*a*) [i.e., $\xi|^{miniat.}_{rect.\,lens} = 6.52 \times 10^{-3}$ when $\rho = 0.84$ - Fig. 11(*a*)]. Moreover, a slight increase of the matching error is obtained when passing to the intermediate [aerodynamic/not-conformal - Fig. 1(*c*)] design by curving the upper part of the lens [$\xi|^{miniat.}_{curve\,lens} = 1.51 \times 10^{-2}$ when $\rho = 0.84$ - Fig. 11(*a*)]. Interestingly, the optimal aerodynamic/conformal arrangement [Fig. 1(*d*)] is not showing a

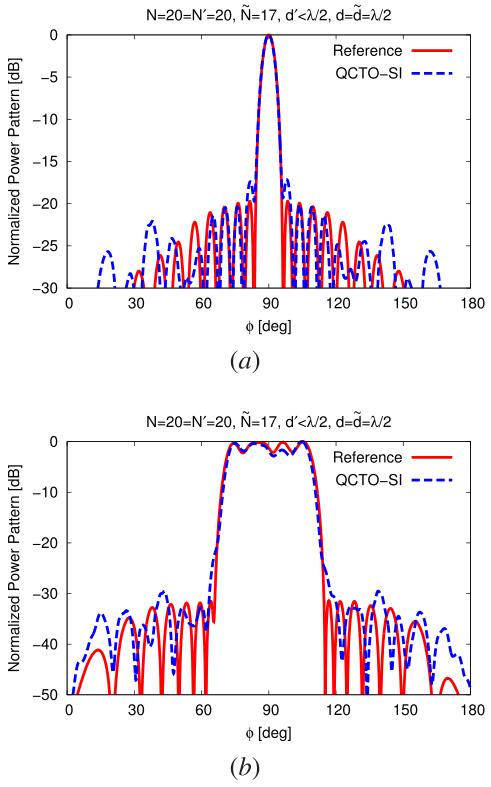

FIGURE 16. ***Numerical Assessment ("Circular-Spline" Radome; $N = 20$, $d = \frac{\lambda}{2}$, $N' = 20$, $d' < \frac{\lambda}{2}$, $\tilde{N} = 17$, $\tilde{d} = \frac{\lambda}{2}$, $\rho = 0.84$; $\phi_s = 90$ [deg])*** **- Power patterns radiated by the *reference* and *QCTO-SI* arrays when considering non-uniform *reference* (*a*) Taylor (*SLL* = 20 [dB]) and (*b*) flat-top excitations.**

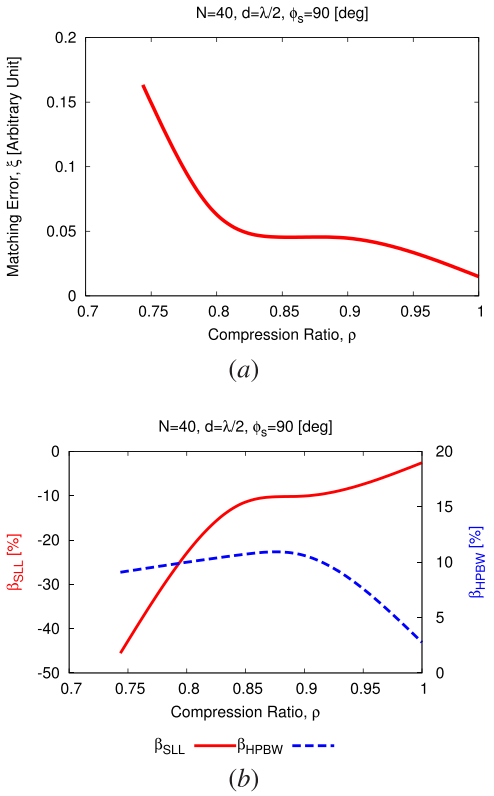

FIGURE 17. ***Numerical Assessment ("Circular-Spline" Radome; $N = 40$, $d = \frac{\lambda}{2}$; $\phi_s = 90$ [deg])*** **- Behaviour of (*a*) the matching error (ξ) and of (*b*) the *SLL* and *HPBW* variation (i.e., β_{SLL} and β_{HPBW}) as a function of the array compression ratio ρ.**

significant increase of the matching error with respect to the two lower-complexity solutions, even if it accounts for a strong deformation of the ground plane in order to match the conformal profile τ_l [Fig. 11(*a*)]. Such outcomes can be further verified by looking at the radiated power patterns shown in Fig. 11(*b*), where it can be observed that the proposed aerodynamic/conformal design slightly differs from the intermediate solutions only in the far sidelobe region. Finally, it is worth observing that the complexity of the synthesized lenses gradually increases, as expected, when passing from the simplest [rectangular - Fig. 1(*b*)] to the most complex [conformal and aerodynamic - Fig. 1(*d*)] layout, as denoted by the plot of the lens permittivity range [Fig. 12(*a*)] and of the anisotropy indexes [Fig. 12(*b*)] versus the array compression ratio. On the other hand, it can be observed that all these designs are characterized by a low complexity in terms of the synthesized excitations through the *SI* procedure, as confirmed by the plot of the *DRR* versus ρ reported in Fig. 12(*c*).

Having assessed the capabilities of the proposed *MbD* methodology for the broadside case, let us now analyze the obtainable solutions when considering a steering of the *reference* pattern. Towards this end, Figure 13 shows the radiated power patterns by the *reference* and *QCTO*$-$*SI* arrangements (still assuming a compression ratio of $\rho = 0.84$) for different

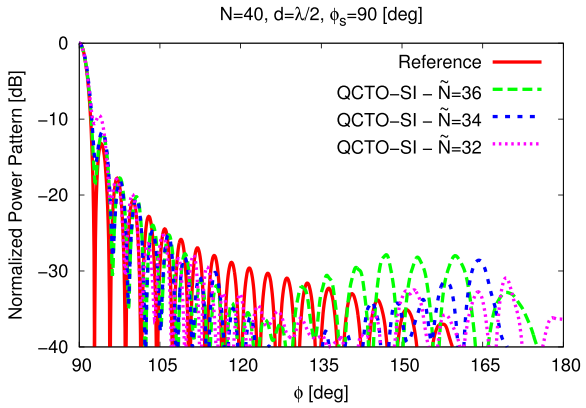

FIGURE 18. ***Numerical Assessment ("Circular-Spline" Radome; $N = 40$, $d = \frac{\lambda}{2}$, $N' = 40$, $d' < \frac{\lambda}{2}$, $\tilde{d} = \frac{\lambda}{2}$; $\phi_s = 90$ [deg])*** **- Power patterns radiated by the *reference* and the *QCTO-SI* arrays when $\tilde{N} = 36$ ($\rho \simeq 0.90$), $\tilde{N} = 34$ ($\rho \simeq 0.85$), and $\tilde{N} = 32$ ($\rho \simeq 0.79$).**

steering angles in the range $90 \leq \phi_s \leq 120$ [deg]. As it can be observed, a very good matching of the *reference* distribution is obtained when considering steering angles $\phi_s \leq 110$ [deg], as verified by the corresponding matching error computed for such a "limit" case (i.e., $\xi|_{\phi_s=110\,[deg]} = 8.60 \times 10^{-2}$, being otherwise $\xi|_{\phi_s=120\,[deg]} = 2.01 \times 10^{-1}$ - Fig. 13). It is worth remarking that shifting the main beam of the

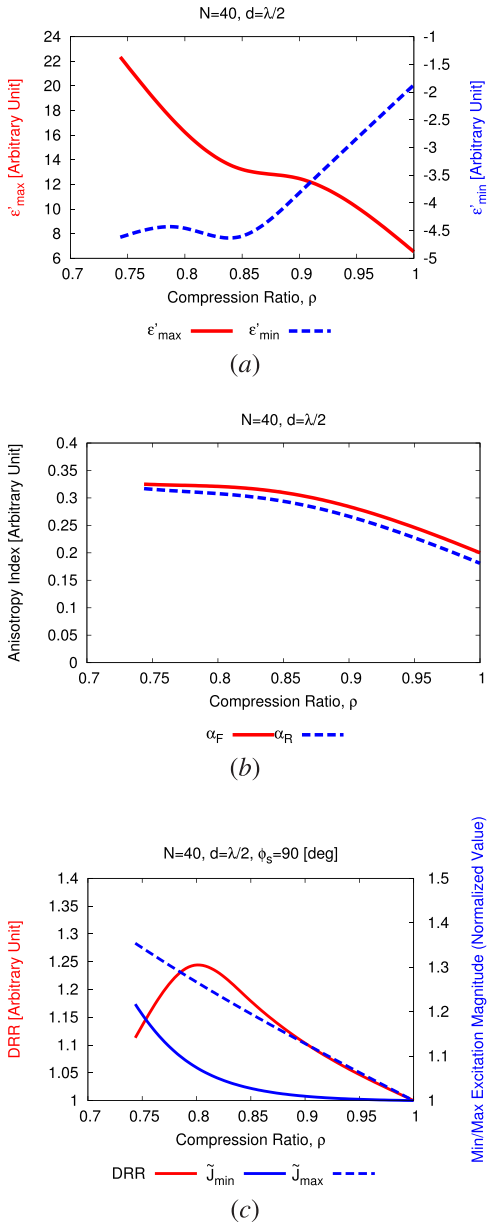

FIGURE 19. *Numerical Assessment* (*"Circular-Spline" Radome*; $N = 40$, $d = \frac{\lambda}{2}$; $\phi_S = 90$ [deg]) - Behavior of (*a*) the bounds of the permittivity tensor (i.e., ε'_{min} and ε'_{max}), (*b*) the anisotropy indexes (i.e., α_F and α_R) of the radome, and (*c*) the descriptors of the synthesized excitations of the *QCTO-SI* array (i.e., $J_{min} = \min_{n=1,\ldots,\tilde{N}} \left|\tilde{J}_n\right|$, $J_{max} = \max_{n=1,\ldots,\tilde{N}} \left|\tilde{J}_n\right|$, and *DRR*) versus the array compression ratio ρ.

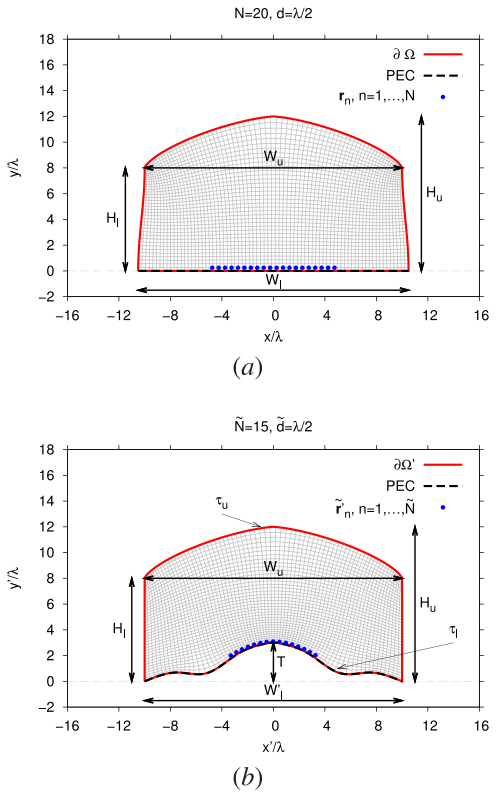

FIGURE 20. *Numerical Assessment* (*"Ogive-Spline" Radome*; $N = 20$, $d = \frac{\lambda}{2}$, $N' = 20$, $d' < \frac{\lambda}{2}$, $\tilde{N} = 15$, $\tilde{d} = \frac{\lambda}{2}$, $\rho = 0.74$) - Geometry, computed transformation grids, and array element positions for the (*a*) *reference* and (*b*) *QCTO-SI* layouts. .

$QCTO - SI$ array does not require a re-design of the conformal metamaterial radome, being obtained by simply re-executing the *SI* step considering a new set of observations of the desired steered far-field pattern (i.e., replacing the entries of the vector $\mathbf{F}$) in solving (9). For completeness, Figure 14 shows the synthesized excitations through the *SI*, indicating that low *DRR* values are always yielded whatever the steering angle [i.e., $1.06 \leq DRR|_{90 \leq \phi_s \leq 120\,[deg]} \leq 1.08$ - Fig. 14(*a*)]. All previous outcomes are confirmed by looking at the plots in Fig. 15, showing the behavior of the matching error [Fig. 15(*a*)], the *SLL* and *HPBW* relative variations [Fig. 15(*b*)] and *SI* excitations properties [$\tilde{J}_{\min}$, $\tilde{J}_{\max}$, and *DRR* - Fig. 15(*c*)] versus the steering angle value.

To further verify that a new execution of the *SI* step allows the $QCTO - SI$ array to reproduce different patterns of the *reference* array, Figure 16 illustrates the radiated power patterns when matching a Taylor pattern with $SLL = 20$ [dB] [Fig. 16(*a*)] and a flat-top pattern from [40]. A very good matching is obtained in both cases, as quantitatively denoted by the computed matching errors [i.e., $\xi|^{Taylor} = 2.03 \times 10^{-2}$ - Fig. 16(*a*), and $\xi|^{Flat-Top} = 9.71 \times 10^{-3}$ - Fig. 16(*b*)]. Such results confirm the potentialities as well as the flexibility of the proposed *MbD* synthesis approach, that enables an easy *reconfigurability* of the miniaturized and conformal architectures without changing the material properties inside Ω'.

To verify the *scalability* of the proposed approach, let us now consider a larger *reference* array, by increasing the number of *TRM*s up to $N = 40$. Figure 17(*a*) shows the behaviour of the matching error versus the compression ratio for such a benchmark. It is worth observing that good matchings (i.e., yielding errors $\xi < 10^{-1}$) are obtained for compression ratios $\rho \geq 0.79$ [being $\tilde{N}\big|_{\rho=0.79} = 32$ - Fig. 17(*a*)], for which limited relative variations of both the *SLL* and *HPBW* [i.e., $\beta_{SLL} > -20\%$ and $\beta_{HPBW} < 10\%$ - Fig. 17(*b*)]

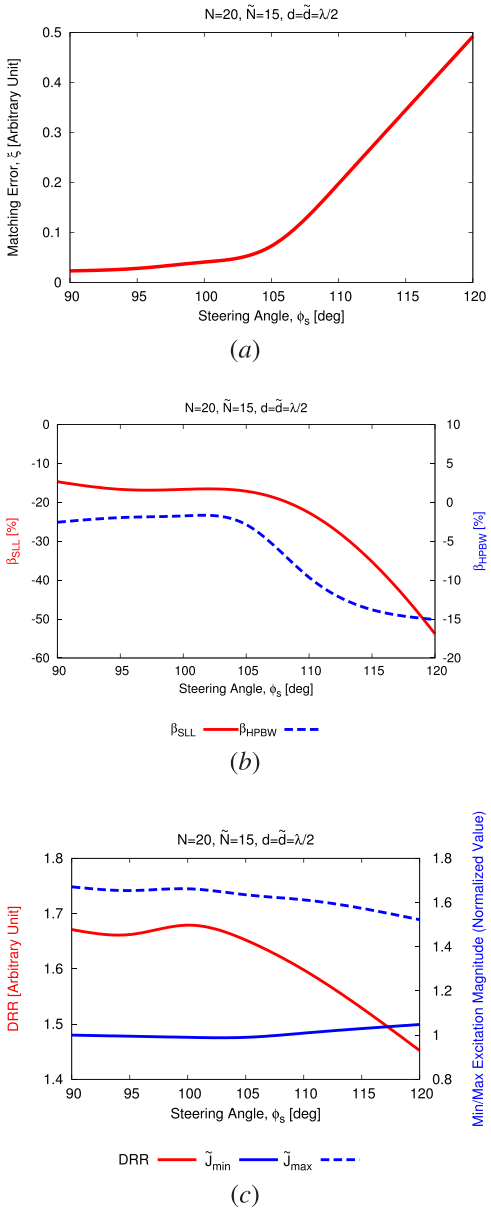

FIGURE 21. ***Numerical Assessment ("Ogive-Spline" Radome; $N = 20$, $d = \frac{\lambda}{2}$, $N' = 20$, $d' < \frac{\lambda}{2}$, $\tilde{N} = 15$, $\tilde{d} = \frac{\lambda}{2}$, $\rho = 0.74$) - Behaviour of (a) the matching error (ξ), (b) the SLL and HPBW variation (i.e., β_{SLL} and β_{HPBW}), and (c) the descriptors of the synthesized excitations of the QCTO-SI array (i.e., $J_{min} = \min_{n=1,\ldots,\tilde{N}} \left|\tilde{J}_n\right|$, $J_{max} = \max_{n=1,\ldots,\tilde{N}} \left|\tilde{J}_n\right|$, and DRR) versus the steering angle ϕ_s.***

can be obtained with respect to the *reference* distribution. To visually verify the "quality" of the obtained solutions, Figure 18 compares the *reference* power pattern with those radiated by $QCTO - SI$ arrangements when letting $\tilde{N} = 36$ ($\xi|_{\rho=0.9} = 4.49 \times 10^{-2}$), $\tilde{N} = 34$ ($\xi|_{\rho=0.85} = 4.55 \times 10^{-2}$), and $\tilde{N} = 32$ ($\xi|_{\rho=0.79} = 6.84 \times 10^{-2}$). Moreover, the overall "complexity" of the designed systems turns out to be acceptable and very close to what has been found for the $N = 20$ case, both in terms of lens permittivity ranges [Fig. 19(a)] and anisotropy [Fig. 19(b)], as well as in terms of synthesized excitations [Fig. 19(c)].

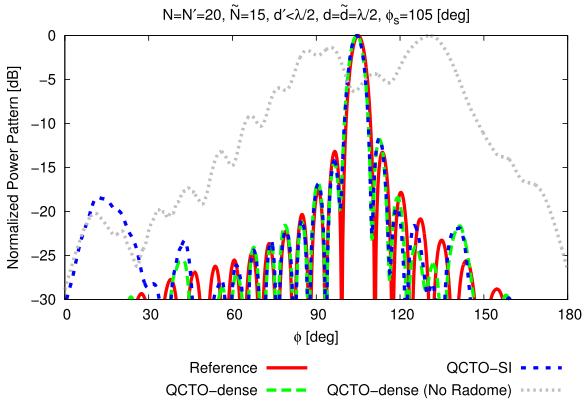

FIGURE 22. ***Numerical Assessment ("Ogive-Spline" Radome; $N = 20$, $d = \frac{\lambda}{2}$, $N' = 20$, $d' < \frac{\lambda}{2}$, $\tilde{N} = 15$, $\tilde{d} = \frac{\lambda}{2}$, $\rho = 0.74$; $\phi_s = 105$ [deg]) - Power patterns radiated by the reference array, the QCTO-dense array (with and without radome), and the QCTO-SI array.***

As a final representative benchmark, let us now consider a different setting of the lens contour ($\partial\Omega'$) involving a visible bending of the miniaturized array in order to fit the underlying profile τ_l shown in Fig. 20(b) (modelled through a symmetric spline curve). Moreover, a different aerodynamic profile has been chosen, by modelling the upper part of $\partial\Omega'$ as a *super-spheroid* radome defined through the following parametric equation [41]

$$\begin{cases} x'(t) = \pm \dfrac{W_u}{2(H_u - H_l)} \times \left[(H_u - H_l)^{\nu} - t^{\nu}\right]^{\frac{1}{\nu}} \\ y'(t) = t + H_l \end{cases} \tag{15}$$

where $t \in [0, (H_u - H_l)]$ and $\nu = 1.4$ (Fig. 20). More in detail, the following geometrical parameters have been considered: $H_u = 12\lambda$, $H_l = 8\lambda$, $W_u = 20\lambda$, $W_l' = 20\lambda$, $T = 3\lambda$, while $W_l = 21\lambda$ [Fig. 20(a)] in order to achieve a compression of the *reference* array [with $N = 20$ elements - Fig. 20(a)] equal to $\rho = 0.74$ [$\tilde{N} = 15$ - Fig. 20(b)]. Figure 21(a) shows the behavior of the far-field matching error versus the steering angle in the range $90 \leq \phi_s \leq 120$ [deg]. As it can be observed, good solutions in terms of matching error are obtained for steering angles $\phi_s \leq 105$ [deg] given the higher deformation of the miniaturized array [i.e., $\xi|_{\phi_s=105\,[deg]} = 7.29 \times 10^{-2}$, being otherwise $\xi|_{\phi_s=110\,[deg]} = 1.97 \times 10^{-1}$ - Fig. 21(a)]. Such a result is confirmed by the plot of β_{SLL} and β_{HPBW} reported in Fig. 21(b) (showing that a good control of both the *SLL* and *HPBW* is achieved up to the "limit" case $\phi_s = 105$ [deg]). Concerning the synthesized excitations through the *SI* step, Figure 21(c) confirms the previous results, by showing that the *DRR* is always low and limited to $1.45 \leq DRR|_{90 \leq \phi_s \leq 120\,[deg]} \leq 1.68$. Moreover, it is worth pointing out that the synthesized lens is characterized by a reduced complexity despite the significant compression ($\rho = 0.74$), as indicated by the ranges of the permittivity tensor (i.e., $\left[\varepsilon'_{\min}, \varepsilon'_{\max}\right] = [-1.13, 9.38]$) as well as by the anisotropy indexes (i.e., $\alpha_F = 2.59 \times 10^{-1}$ and $\alpha_R = 2.36 \times 10^{-1}$). In order to understand the effectiveness of the synthesis methodology, the power

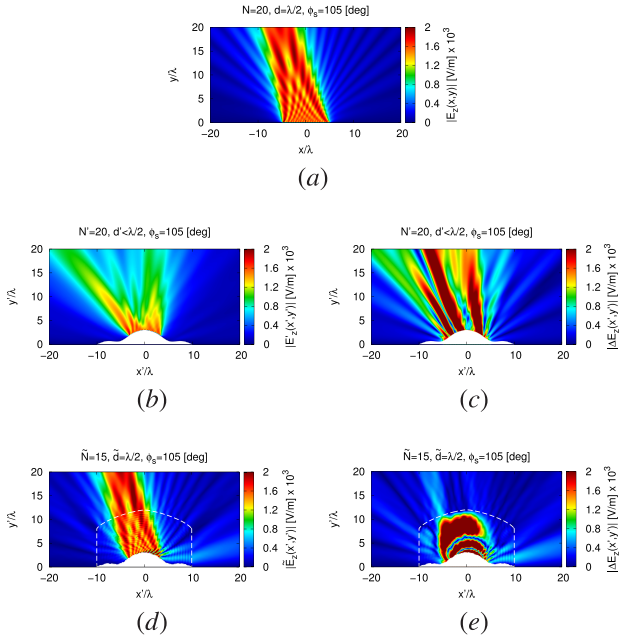

FIGURE 23. ***Numerical Assessment*** **(*"Ogive-Spline" Radome*; $N = 20$, $d = \frac{\lambda}{2}$, $N' = 20$, $d' < \frac{\lambda}{2}$, $\tilde{N} = 15$, $\tilde{d} = \frac{\lambda}{2}$, $\rho = 0.74$; $\phi_S = 105$ [deg]) - Magnitude of near-field radiated by the (*a*) *reference* array, (*b*) *QCTO-dense* array without radome, and (*c*) *QCTO-SI* array; magnitude of the near-field difference between the *reference* and (*c*) the *QCTO-dense,* and (*e*) the *QCTO-SI* distributions. .**

patterns radiated by the $QCTO - dense$ and $QCTO - SI$ arrangements are compared to that of the *reference* array when considering the identified "limit" steering angle (i.e., $\phi_s = 105$ [deg] - Fig. 22). If from the one hand such a plot verifies the capability of the $QCTO - SI$ arrangement in reproducing the *reference* field pattern, on the other hand it clearly shows that bending and compressing the reference elements causes a severe degradation/defocusing of the radiated field pattern without using the metamaterial coating (i.e., the $QCTO - dense$ array in the "no-radome" scenario - Fig. 22). For completeness, the near-field distributions are reported in Fig. 23, where it can be observed that the $QCTO - SI$ layout radiates a field distribution outside $\partial\Omega'$ very close to that of the *reference* array [Fig. 23(d) vs. Fig. 23(a), the difference field being shown in Fig. 23(e)], while the $QCTO - dense$ array is unable to focus the beam when removing the *QCTO* lens [Fig. 23(b) vs. Fig. 23(a) and the difference field in Fig. 23(c)].

IV. CONCLUSIONS

In this work, the design of high performance conformal radiating structures has been addressed within the *MbD* paradigm. A novel synthesis methodology has been proposed, effectively combining a generalized *QCTO* approach [28] and a *SVD*-based *SI* strategy [3] to deal with

- the reduction of the aperture (L) and number of *TRM*s (N) of a large *reference* array in order to match it to the hosting structure while keeping unaltered its radiation performances;
- the synthesis of a metamaterial radome whose shape is fully controllable by the designer and conformal to arbitrarily-shaped mechanical supports.

A set of representative results - carefully selected from an exhaustive numerical validation - has been shown in order to verify the effectiveness and the current limitations of the proposed *MbD* methodology. Such an analysis has pointed out that

1) a reduction of the antenna aperture and number of elements can be achieved without introducing significant degradations in the radiated field;
2) unlike previous *QCTO*-based designs [3], a conformal shaping of the final antenna-lens radiating structure can be easily achieved;
3) a clear trade-off exists between the compression of the *reference* array and the complexity of the synthesized lenses, both in terms of permittivity/permeability ranges and anisotropy;
4) the proposed methodology is flexible and scalable, allowing to handle the transformation of *reference* layouts with different dimensions (N), having non-uniform excitations, arbitrary *SLL* and *HPBW*, as well as smaller/larger values of the inter-element spacing d.

Future works, beyond the actual goals of this paper, will be addressed towards the extension of the developed *MbD* synthesis approach to deal with full *3-D* systems. Moreover, the possibility to integrate the design into an optimization loop to synthesize lenses with reduced anisotropy will be investigated, by considering the exploitation of fast *EM* solvers or properly defined *surrogate* models [25]. An experimental assessment is envisaged, as well, by identifying suitable fabrication technologies in order to realize the synthesized metamaterial coatings.

REFERENCES

[1] R. J. Mailloux, *Phased Array Antenna Handbook*, 2nd ed. Norwood, MA, USA: Artech House, 2005.
[2] P. Rocca, G. Oliveri, R. J. Mailloux, and A. Massa, "Unconventional phased array architectures and design methodologies—A review," *Proc. IEEE*, vol. 104, no. 3, pp. 544–560, Mar. 2016.
[3] G. Oliveri, E. T. Bekele, M. Salucci, and A. Massa, "Array miniaturization through QCTO-SI metamaterial radomes," *IEEE Trans. Antennas Propag.*, vol. 63, no. 8, pp. 3465–3476, Aug. 2015.
[4] G. A. Thiele and C. Donn, "Design of a small conformal array," *IEEE Trans. Antennas Propag.*, vol. 22, no. 1, pp. 64–70, Jan. 1974.
[5] J. J. Yu and S. Lim, "Design of multi-band, compact parasitic array with twisted, helical directors," *IEEE Trans. Antennas Propag.*, vol. 61, no. 1, pp. 444–449, Jan. 2013.
[6] K. Boyle, "Radiation patterns and correlation of closely spaced linear antennas," *IEEE Trans. Antennas Propag.*, vol. 50, no. 8, pp. 1162–1165, Aug. 2002.
[7] L. Peng, L. Ran, Y. K. Zou, and J. A. Kong, "A miniaturized phased array aperture antenna based on bulk ferroelectric material," *Microw. Opt. Technol. Lett.*, vol. 49, no. 1, pp. 37–40, Jan. 2007.
[8] R. L. Haupt, "Thinned arrays using genetic algorithms," *IEEE Trans. Antennas Propag.*, vol. 42, no. 7, pp. 993–999, Jul. 1994.
[9] L. Poli, P. Rocca, M. Salucci, and A. Massa, "Reconfigurable thinning for the adaptive control of linear arrays," *IEEE Trans. Antennas Propag.*, vol. 61, no. 10, pp. 5068–5077, Oct. 2013.

[10] G. Oliveri, L. Manica, and A. Massa, "ADS-based guidelines for thinned planar arrays," *IEEE Trans. Antennas Propag.*, vol. 58, no. 6, pp. 1935–1948, Jun. 2010.

[11] G. Oliveri, M. Donelli, and A. Massa, "Linear array thinning exploiting almost difference sets," *IEEE Trans. Antennas Propag.*, vol. 57, no. 12, pp. 3800–3812, Dec. 2009.

[12] P. Rocca, M. Benedetti, M. Donelli, D. Franceschini, and A. Massa, "Evolutionary optimization as applied to inverse scattering problems," *Inverse Prob.*, vol. 25, no. 12, pp. 1–41, Dec. 2009.

[13] D. Sartori, G. Oliveri, L. Manica, and A. Massa, "Hybrid design of non-regular linear arrays with accurate control of the pattern sidelobes," *IEEE Trans. Antennas Propag.*, vol. 61, no. 12, pp. 6237–6242, Dec. 2013.

[14] A. Massa, P. Rocca, and G. Oliveri, "Compressive sensing in electromagnetics—A review," *IEEE Antennas Propag. Mag.*, vol. 57, no. 1, pp. 224–238, Feb. 2015.

[15] G. Oliveri and A. Massa, "Bayesian compressive sampling for pattern synthesis with maximally sparse non-uniform linear arrays," *IEEE Trans. Antennas Propag.*, vol. 59, no. 2, pp. 467–481, Feb. 2011.

[16] F. Viani, G. Oliveri, and A. Massa, "Compressive sensing pattern matching techniques for synthesizing planar sparse arrays," *IEEE Trans. Antennas Propag.*, vol. 61, no. 9, pp. 4577–4587, Sep. 2013.

[17] G. Oliveri, E. T. Bekele, F. Robol, and A. Massa, "Sparsening conformal arrays through a versatile *BCS*-based method," *IEEE Trans. Antennas Propag.*, vol. 62, no. 4, pp. 1681–1689, Apr. 2014.

[18] W. Zhang, L. Li, and F. Li, "Reducing the number of elements in linear and planar antenna arrays with sparseness constrained optimization," *IEEE Trans. Antennas Propag.*, vol. 59, no. 8, pp. 3106–3111, Aug. 2011.

[19] D. H. Werner and D.-H. Kwon, Eds., *Transformation Electromagnetics and Metamaterials: Fundamental Principles and Applications*. New York, NY, USA: Springer, 2014.

[20] D.-H. Kwon and D. H. Werner, "Transformation electromagnetics: An overview of the theory and applications," *IEEE Antennas Propag. Mag.*, vol. 52, no. 1, pp. 24–46, Feb. 2010.

[21] H. Chen, C. T. Chan, and P. Sheng, "Transformation optics and metamaterials," *Nature Mater.*, vol. 9, pp. 387–396, May 2010.

[22] G. Oliveri, D. H. Werner, and A. Massa, "Reconfigurable electromagnetics through metamaterials—A review," *Proc. IEEE*, vol. 103, no. 7, pp. 1034–1056, Jul. 2015.

[23] C. Lu, Z. L. Mei, W. X. Tang, and T. J. Cui, "Manipulating scattering features by metamaterials," *EPJ Appl. Metamater.*, vol. 3, p. 3, Mar. 2016.

[24] J. B. Pendry, D. Schurig, and D. R. Smith, "Controlling electromagnetic fields," *Science*, vol. 312, pp. 1780–1782, Jun. 2006.

[25] A. Massa, G. Oliveri, P. Rocca, and F. Viani, "System-by-design: A new paradigm for handling design complexity," in *Proc. Eur. Conf. Antennas Propag.*, Apr. 2014, pp. 1423–1426.

[26] G. Oliveri, E. T. Bekele, M. Salucci, and A. Massa, "Transformation electromagnetics miniaturization of sectoral and conical metamaterial-enhanced horn antennas," *IEEE Trans. Antennas Propag.*, vol. 64, no. 4, pp. 1508–1513, Apr. 2016.

[27] G. Oliveri, F. Viani, N. Anselmi, and A. Massa, "Synthesis of multilayer WAIM coatings for planar-phased arrays within the system-by-design framework," *IEEE Trans. Antennas Propag.*, vol. 63, no. 6, pp. 2482–2496, Jun. 2015.

[28] G. Oliveri, E. T. Bekele, D. H. Werner, J. P. Turpin, and A. Massa, "Generalized QCTO for metamaterial-lens-coated conformal arrays," *IEEE Trans. Antennas Propag.*, vol. 62, no. 8, pp. 4089–4095, Aug. 2014.

[29] M. Salucci, G. Oliveri, N. Anselmi, G. Gottardi, and A. Massa, "Performance enhancement of linear active electronically scanned arrays by means of *MbD*-synthesized metalenses," *J. Electromagn. Waves Appl.*, vol. 32, no. 8, pp. 927–955, Dec. 2017.

[30] D.-H. Kwon, "Quasi-conformal transformation optics lenses for conformal arrays," *IEEE Antennas Wireless Propag. Lett.*, vol. 11, pp. 1125–1128, 2012.

[31] G. Oliveri, L. Tenuti, E. Bekele, M. Carlin, and A. Massa, "An SbD-QCTO approach to the synthesis of isotropic metamaterial lenses," *IEEE Antennas Wireless Propag. Lett.*, vol. 13, pp. 1783–1786, 2014.

[32] Y. Luo, J. Zhang, L. Ran, H. Chen, and J. A. Kong, "New concept conformal antennas utilizing metamaterial and transformation optics," *IEEE Antennas Wireless Propag. Lett.*, vol. 7, pp. 509–512, 2008.

[33] R. C. Mitchell-Thomas, O. Quevedo-Teruel, T. M. McManus, S. A. R. Horsley, and Y. Hao, "Lenses on curved surfaces," *Opt. Lett.*, vol. 39, no. 12, pp. 3551–3554, Jun. 2014.

[34] Y. Jang, M. Yoo, and S. Lim, "Conformal metamaterial absorber for curved surface," *Opt. Exp.*, vol. 21, no. 20, pp. 24163–24170, Oct. 2013.

[35] S. Sajuyigbe, B. J. Justice, A. F. Starr, and D. R. Smith, "Design and analysis of three-dimensionalized ELC metamaterial unit cell," *IEEE Antennas Wireless Propag. Lett.*, vol. 8, pp. 1268–1271, 2009.

[36] T. D. Karamanos, A. I. Dimitriadis, and N. V. Kantartzis, "Compact double-negative metamaterials based on electric and magnetic resonators," *IEEE Antennas Wireless Propag. Lett.*, vol. 11, pp. 480–483, 2012.

[37] A. Rivas, J. A. Rodriguez, F. Ares, and E. Moreno, "Planar arrays with square lattices and circular boundaries: Sum patterns from distributions with uniform, amplitude or very low dynamic-range ratio," *IEEE Antennas Propag. Mag.*, vol. 43, no. 5, pp. 90–93, Oct. 2001.

[38] G. K. Mahanti, S. Das, and A. Chakraborty, "Design of phase-differentiated reconfigurable array antennas with minimum dynamic range ratio," *IEEE Antennas Wireless Propag. Lett.*, vol. 5, no. 1, pp. 262–264, Dec. 2006.

[39] J. Hunt *et al.*, "Broadband wide angle lens implemented with dielectric metamaterials," *Sensors*, vol. 11, no. 8, pp. 7982–7991, 2011.

[40] T. Isernia, O. M. Bucci, and N. Fiorentino, "Shaped beam antenna synthesis problems: Feasibility criteria and new strategies," *J. Electromagn. Waves Appl.*, vol. 12, no. 1, pp. 103–137, 1998.

[41] P. L. Overfelt, "Superspheroids: A new family of radome shapes," *IEEE Trans. Antennas Propag.*, vol. 43, no. 2, pp. 215–220, Feb. 1995.

MARCO SALUCCI received the M.S. degree in telecommunication engineering from the University of Trento, Italy, in 2011, and the Ph.D. degree in information and communication technology from the International Doctoral School, Trento, in 2014. From 2014 to 2016, he was a Post-Doctoral Researcher with CentraleSupélec, involved in the SIRENA project through DIGITEO, France, from 2014 to 2017. From 2016 to 2017, he was a Post-Doctoral Researcher with the Commissariat à l'énergie atomique et aux énergies alternatives, France. He is currently a Post-Doctoral Researcher with the Department of Information Engineering and Computer Science, University of Trento, Italy, and a member of the ELEDIA Research Center. Moreover, in 2014, he was the Technical Director of the ELEDIA Offshore-Lab @ Laboratoire des Signaux et Systèmes. He was a member of the COST Action TU1208 Civil Engineering Applications of Ground Penetrating Radar He is a member of the IEEE Antennas and Propagation Society. He serves as a Reviewer for different international journals, including the IEEE TRANSACTIONS ON ANTENNAS AND PROPAGATION, the IEEE ANTENNAS AND WIRELESS PROPAGATION LETTERS, the IEEE JOURNAL ON MULTISCALE AND MULTIPHYSICS COMPUTATIONAL TECHNIQUES, and *IET on Microwaves, Antennas and Propagation*.

His research activities are mainly concerned with inverse scattering, GPR microwave imaging techniques, antenna synthesis, and computational electromagnetics with focus on system-by-design methodologies integrating optimization techniques, and learning-by-examples methods for real-world applications.

GIACOMO OLIVERI (SM'13) received the B.S. and M.S. degrees in telecommunications engineering and the Ph.D. degree in space sciences and engineering from the University of Genoa, Italy, in 2003, 2005, and 2009, respectively. He is currently a Tenure Track Associate Professor with the Department of Information Engineering and Computer Science, University of Trento, and a member of the ELEDIA Research Center. Moreover, he is also an Adjunct Professor with the CentraleSupélec, Gif-sur-Yvette, France, and also a member of the Laboratoire des signaux et systèmes (L2S), CentraleSupélec. He was a Visiting Researcher with L2S in 2012, 2013, and 2015, and an Invited Associate Professor with the University of Paris Sud, France, in 2014.

He has authored or co-authored of over 330 peer reviewed papers on international journals and conferences. His research work is mainly focused on electromagnetic direct and inverse problems, system-by-design and metamaterials, and antenna array synthesis. He serves as an Associate Editor of the IEEE Antennas and Wireless Propagation Letters, the IEEE Journal on Multiscale and Multiphysics Computational Techniques, the *International Journal of Antennas and Propagation*, the *International Journal of Distributed Sensor Networks*, and the *Microwave Processing* journal. He is the Chair of the IEEE AP/ED/MTT North Italy Chapter.

NICOLA ANSELMI received the master's degree in telecommunication engineering from the University of Trento, Italy, in 2012, and the Ph.D. degree in information and communication technology from the International Doctoral School, Trento, Italy, in 2018. Since 2012, he has been a member of the ELEDIA Research Center and also has been a member of the IEEE Antennas and Propagation Society. Since 2014, he is serving as a Reviewer for different international journals, including the IEEE Transactions on Antennas and Propagation, the IEEE Antennas and Wireless Propagation Letters, and *IET on Microwaves, Antennas & Propagation*. He was a recipient of the Giorgio Barzilai Award for Young Researchers by the Italian Electromagnetic Society in 2016.

His research activities are mainly focused on synthesis methods for unconventional antenna array architectures, tolerance analysis of antenna systems, and electromagnetic inverse scattering techniques, with interest on compressive sensing methodologies for microwave imaging applications.

ANDREA MASSA (F'17) received the Laurea degree in electronic engineering and the Ph.D. degree from the EECS, University of Genoa, Genoa, Italy, in 1992 and 1996, respectively. From 1997 to 1999, he was an Assistant Professor of electromagnetic fields with the Department of Biophysical and Electronic Engineering, University of Genoa. From 2001 to 2004, he was an Associate Professor with the University of Trento. Since 2005, he has been a Full Professor of electromagnetic fields with the University of Trento, where he currently teaches electromagnetic fields, inverse scattering techniques, antennas and wireless communications, wireless services and devices, and optimization techniques.

He is currently the Director of the network of federated laboratories ELEDIA Research Center [ELEDIA@UTB, Bandar Seri Begawan, Brunei, ELEDIA@UESTC, Chengdu, China, ELEDIA@USIL in Lima, Perù, ELEDIA@UniNAGA, Nagasaki, Japan, ELEDIA@L2S, Paris, France, ELEDIA@CTU, Prague, Czech Republic, ELEDIA@UniTN, Trento, Italy, ELEDIA@TSINGHUA, Beijing, China, and ELEDIA@Innov'COM, Tunis, Tunisia]. Moreover, he is also an Adjunct Professor with Penn State University, USA, also a Professor with the CentraleSupélec, France, and also the UC3M-Santander Chair of Excellence with the Universidad Carlos III de Madrid, Spain. He has been holder of a Senior DIGITEO Chair with the L2S-CentraleSupélec and CEA LIST, Saclay, France, a Visiting Professor with the Missouri University of Science and Technology, USA, Nagasaki University, Japan, the University of Paris Sud, France, Kumamoto University, Japan, and the National University of Singapore, Singapore. He has been appointed the IEEE AP-S Distinguished Lecturer from 2016 to 2018. He serves as an Associate Editor of the IEEE Transaction on Antennas and Propagation and the *International Journal of Microwave and Wireless Technologies* and is a member of the Editorial Board of the *Journal of Electromagnetic Waves and Applications*, a permanent member of the PIERS Technical Committee and the EuMW Technical Committee, and a ESoA member. He has been appointed in the Scientific Board of the Società Italiana di Elettromagnetismo and elected in the Scientific Board of the Interuniversity National Center for Telecommunications. He has been appointed in 2011 by the National Agency for the Evaluation of the University System and National Research as a member of the Recognized Expert Evaluation Group (Area 09, Industrial and Information Engineering) for the evaluation of the researches at the Italian University and Research Center from 2004 to 2010. Furthermore, he has been elected as the Italian Member of the Management Committee of the COST Action TU1208—Civil Engineering Applications of Ground Penetrating Radar. His research activities are mainly concerned with inverse problems, analysis/synthesis of antenna systems and large arrays, radar systems synthesis and signal processing, cross-layer optimization and planning of wireless/RF systems, semantic wireless technologies, system-by-design and material-by-design (metamaterials and reconfigurable-materials), and theory/applications of optimization techniques to engineering problems (tele-communications, medicine, and biology).

He has authored or co-authored over 700 scientific publications among which about 300 on international journals and over 450 in international conferences where he presented over 150 invited contributions. He has organized over 70 scientific sessions in international conferences and has participated on several technological projects in the European framework (20 EU Projects) and at the national and local level with national agencies (over 150 Projects/Grants). He is an IET Fellow and Electromagnetic Academy Fellow).